Biodome Systems for Enhanced Bone and Tissue Regeneration

A thesis submitted by

Brooke Longo

In partial fulfillment of the requirements for the degree of

Master of Science

in

Biomedical Engineering
Tufts University

February 2025

Advisor: Dr. David Kaplan

Abstract:

Limb regeneration is an expanding focus of biomedical science due to the rise in the number of individuals suffering from the loss of a limb. Non-regenerative mammalian models, such as rodents, are invaluable research subjects for whole limb regeneration and functional restoration, as adult animals show many similarities in wound healing to humans. In this thesis, I propose the use of multiple forms of non-invasive stimulation methods, e.g. optical stimulation in the form of photobiomodulation, to enhance regenerative capabilities in non-regenerative species. To do this, I created devices to test this method in vitro and in vivo. In vitro systems focused on applying the proposed treatment methods to human mesenchymal stem cells (hMSCs) via 3D printed LED arrays with fixed 810 nm LEDs. While the in vivo system was comprised of a multifaceted wearable device to promote the regeneration process of an amputated CD-1 mouse digit. The system is composed of a custom-made 810 nm induction diode that is fixed within a 3D printed wearable protective cast, which allows for wireless optical treatment at the amputation site. In addition to a wearable device, a secondary system comprised of an array of 810 nm diodes is used to continue treatment after removal of the wearable device. The initial results of both in vitro and in vivo studies indicate that the treatment with 810 nm near infrared light upregulates bone morphogenetic protein 2 (BMP2) expression, which plays a role in bone formation, as well as improves healing around the wound site. The second component of this system focuses on electrical stimulation to further stimulate wound healing. Devices to generate electric fields have been developed using 3D printed guides and super-conductive 101 copper plates. The initial results indicate potential migration and enhancement in cell proliferation.

Key Words: Tissue regeneration, bone regeneration, wound healing, wearable devices, near-infrared (NIR) light treatment, photobiomodulation, electric field (EF) stimulation, 3D printing

Acknowledgements

The following work was made possible through collaboration with numerous individuals from both academia and industry. Firstly, I would like to acknowledge my advisor Dr. David Kaplan. It was truly an honor getting to work with you and your group not only on this project but on many more across your incredibly diverse lab. From being your lab tech to being your student, thank you for the amazing and educational journey you allowed me to embark on. Working with you has broadened my knowledge to realms I didn't even imagine I would adventure into and has allowed me to deepen my love for this field of study.

Next, I would like to thank my thesis committee for being willing to accept and participate in my defense on such short notice. I would like to give a special thank you to Dr. James Intriligator who was a true all-star for joining in what was truly the eleventh hour. Not only did you accept the role of committee member, but you truly went above and beyond with your interest in the subject matter and eye-opening ideas for future study.

I would also like to give a very special thank you to Dr. Chunmei Li. All of the work done in this paper would truly not be possible without you. It has been a true pleasure and honor getting to work with and learn from you as much as I have. You are an incredibly knowledgeable and an overall amazing person to work with and I am happy I can call you my colleague and friend.

I would also like to give a big thank you to all my BME lab mates for their support and help through numerous aspects of this project, especially Edward, Liam, Vincent, Glenn, and Giles. Thank you to my mom, aunt, and the rest of my family and friends for your constant support and encouragement throughout my time at Tufts. And a very special thank you to my amazing partner who was always there for me day and night for all the ups and downs that come with completing a thesis. Without you I don't think I would be where I am today. Your constant support,

encouragement, and love have made a world of difference in my life. Lastly, I want to thank Skipper (our dog) for having no idea why mommy was an emotional mess but accepting all the suffocating snuggles she needed to get through tough days anyway.

Table of Contents

List of Figures

List of Tables

Chapter 1: Introduction

1.1 Background

In the United States approximately 2.1 million people suffer from the loss of a limb[1]. Limb loss can occur for a variety of different reasons, from illness to accident, with the number of individuals afflicted steadily increasing[1,2]. Not only does losing a limb affect the amputee's ability to function normally, 36% of amputees suffer from depression related to limb loss[1]. Currently, prosthetic limbs are the go-to solution for those suffering the loss of a limb. Though the technology for prosthetic limbs has continued to increase significantly over past years, from simple metal structures to advanced 3D printed and robotic appendages[3,4], there unfortunately is still no ideal solution that meets all amputee physical and mental needs.

Currently, there are a number of different options available to address limb loss and each comes with its strengths and limitations. Traditional prosthetics are widely used amongst amputees, with a variety of tools for attachment to help the individual perform basic functions (e.g., grippers for holding household objects). Unfortunately, traditional prosthetics can cause discomfort and irritation at the stump site. Additionally, in younger amputees, traditional prosthetics are outgrown quickly resulting in the need for multiple devices to be purchased, which can be very costly. Traditional prosthetics also lack the ability to provide sensory feedback, which can be a critical component for the amputee as it has been shown to increase functionality as well as decreased phantom limb pain[5]. 3D printed prosthetics have improved aspects over traditional prosthetics by reducing costs and allowing for scaling with growing amputees, while still maintaining basic functions[3]. However, like traditional prosthetics, 3D printed prosthetics can also cause discomfort at the stump as well as provide an unnatural appearance. Alternatively, robotic prosthetics allow wearers to achieve higher levels of function and also receive sensory feedback[5].

However, these prosthetics typically come with a higher price tag and can have long-term discomfort at the stump.

Regenerative medicine approaches for limb loss have been studied in non-regenerative models with the addition of pharmaceuticals[6], optical stimulation[7–9], electrical stimulation[10–13], mechanical stimulation[14], and biomaterial implantation[15], among others. Each method offers some promise in aiding the regenerative process; however, none of these approaches have resulted in full-scale limb regrowth and functionality in an adult non-regenerative species. Thus, a combination approach may be best towards improving success toward full-scale limb regeneration.

Our goal is to generate a multi-stimulation wearable device to support limb regeneration. The device incorporates a protective cast that encompasses the damaged limb and a soft sleeve that delivers a pharmaceutical cocktail, in combination with three forms of external stimulation (optical, electrical, mechanical). The addition of these external stimuli aids in regenerative process[6–14]. The current method would be a completely internalized system with all three subsystems built directly into the biodome protective cast. Combining these three forms of wound stimulation with our current biodome, a pharmaceutical hydrogel that directly attaches to the amputation site, is hypothesized to support improved tissue regeneration. The following work describes the initial steps toward this goal with a focus on designing and testing the optical and electrical stimulation methods.

1.2 Thesis Objective

The objective of this thesis is to generate the second phase of our Biodome system that makes use of additional forms of stimulation, optical and electrical, with our already existing pharmaceutical delivery system. The first addition uses near infrared light (NIR) to aid in regeneration. We tested our proposed treatment in an in vitro model using human mesenchymal

stem cells (hMSCs). In vitro testing was done to confirm that the treatment was both safe and induced an enhanced osteogenic effect on the cells. Accelerated regeneration was initially pursued by making use of the interaction of low-intensity 810 nm wavelength light with the core circadian clock protein cryptochrome 1 (CRY1). Peng et al. (2022) showed that exposure to 810 nm light reduced CRY1 levels, which in turn resulted in the activation of bone morphogenic protein (BMP) signaling pathways and promoted osteogenesis[7]. This approach was initially chosen because it is a noninvasive, optical approach to aid bone regeneration. The second addition was the use of electric fields (EF) to aid in tissue regeneration and cell migration to the wound site[11]. Electric fields have been shown to enhance numerous aspects of wound healing, e.g. nerve regeneration[11,12]. Manipulation of these EFs is ideal for our goals as it is a non-invasive variant of electrical stimulation that can be easily added to our overall system.

Chapter 2: Optical Stimulation for Regeneration

2.1 Introduction

Optical treatment, or photobiomodulation, is a non-invasive form of light therapy that makes use of different wavelengths of light to provide therapeutic effects to patients, such as arthritis relief or vascular issues[16–18]. The wavelength of light chosen for treatment directly impacts the type of therapy and the penetration depth of the light itself. Light in the Near InfraRed (NIR) range, specifically from 650 – 950 nm, has deeper penetration depth due to the decreased absorption and scattering of biological tissue in this range making it advantageous for treating deeper tissues[19]. This spectrum is ideal for our work as it allows our applied treatment to interact not only at the superficial level of the wound site but also at the innermost bone level.

Previous work in the field has shown promise with the use of 810 nm wavelength light specifically[7]. In the work of Peng et. al, the authors were able to show accelerated bone regeneration in a rat model with the application of 810 nm NIR light as well as a potential mechanism through in vitro studies[7]. Based on their in vitro work, they believed that the promoted osteoblast differentiation was related to a reduction in cryptochrome 1 (CRY1) brought on by the exposure to NIR light treatment[7]. They noted that the reduction of CRY1 activated other pro-osteogenic differentiation pathways, like bone morphogenic protein (BMP), and showed higher levels of additional osteogenic markers, like Runx2[7]. Figure 1 below shows an illustration of the proposed mechanism. In this mechanism, the NIR light is promoting ubiquitination of CRY1 within the nucleus due to sodium influx related to NIR light interaction with the *Scn4a* gene. This reduction of CRY1 results in an increase in osteogenic differentiation.

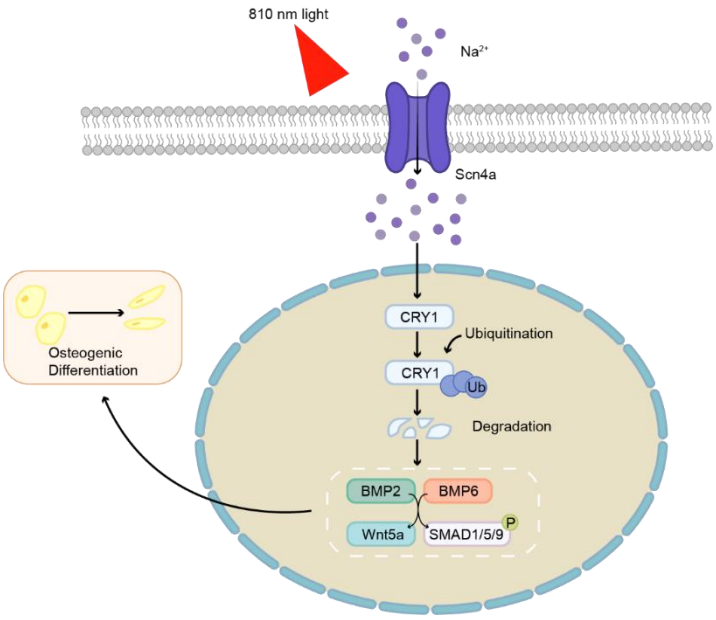

Figure 1: Schematic of NIR light interaction at the cellular level resulting in a possible mechanism for CRY1 reduction and promoted osteogenesis.

To better understand this proposed mechanism, understanding CRY1 at a more fundamental level is necessary. In a 24-hour period, the bodies' daily physiological rhythms and behaviors are controlled by the circadian clock[20]. This control is achieved in part via feedback loops involving clock proteins. One family of clock proteins that play a critical role in regulating circadian rhythms are the CRY proteins. In particular, CRY1 has been shown to have a regulatory relationship with certain biological pathways, e.g. the cyclic Adenosine monophosphate (cAMP)/ protein kinase A system (PKA) signaling pathway[21]. In instances with reduced CRY1 levels, studies have shown that the cAMP/PKA signaling pathway becomes activated[21]. Activation of this pathway has in turn been shown to increase expression of osteogenic related genes like BMP2 and Runx2[22,23]. Expression of both BMP2 and Runx2 is critical as both genes play a major role in inducing osteogenic differentiation of mesenchymal stem cells and mediating osteoblast differentiation while also regulating osteoclast differentiation[24–26]. Gaining the ability to modulate

the expression levels of these genes would allow in theory for greater affinity to osteogenic differentiation in cells and in turn a theoretical option to promote bone regeneration.

In this chapter, the goal was to build upon the work of Peng et. al. This was accomplished by developing a device that would allow us to administer 810 nm NIR light to cultured human mesenchymal stem cells (hMSCs). Through further analysis, we aimed to determine if we can manipulate the levels of CRY1 expression as well as the subsequent expression of pathways and genes related to osteogenesis. In addition to in vitro studies, preliminary in vivo studies have been conducted to determine the effectiveness of the treatment in a limb amputation CD-1 mouse model.

2.2 Device Overview – in vitro

2.2.1 System Design and Fabrication

In vitro studies required the development of a device that allowed NIR light treatment to be administered to each well of a well plate (48 or 6) individually. To accomplish this, a custom LED outfitted well plate covers (Figure 2) were designed in Solidworks (Dassault Systemes, Waltham, MA) and printed using a Prusa MK3S+ 3D printer (Prusa Research, Prague, Czech Republic) out of transparent polylactic acid (PLA) (Sunlu). The outer dimensions of the custom well plate cover are 137.5 mm long, 95.5 mm wide, and 32 mm high. The inner dimensions are 127.75 mm long, 85.75 mm wide, and 30.5 mm high. The holes for the LEDs are dimensioned to 5.1 mm to provide a snug fit for the 810 nm LEDs (Digikey) as well as allow for easy swapping for blow outs or alternative wavelength testing. Well plate covers were made for both 48 and 6 well plates, with the distribution of the LEDs based upon the specific well plate. Both plate covers were printed from transparent PLA on a Prusa MK3S+. Transparent PLA was chosen due to its innate ability to scatter light. By scattering light with these covers it allows for the maximum exposure to be achieved. For 48 well plate covers, a total of twelve 810 nm LEDs were used for

treatment of twelve wells. For each well, one 5.1 mm LED hole was placed in direct alignment with one well, as the diameter of the LED is approximately equivalent to the diameter of the well diameter (Figure 2a). While for 6 well plate covers, five 5.1 mm LED holes were patterned per one well (Figure 2b). This configuration was chosen as it was the most even distribution with the least number of LEDs used that accommodated the diameter of the well. In addition to the LED plate covers, two solid plate covers (Figure 2c) with identical dimensions were also 3D printed out of black filament (Hatchbox) to be used for the control group. Black PLA was chosen as black is a natural light absorber. By shielding the control plates in a light absorbing color material, we were able to assure that the control plates were not receiving any light exposure during the treatment period. Power (1.80 V, 0.4A) was provided to the LEDs by a Hanmatek 305T power supply (Hanmatek, Shenzhen, China).

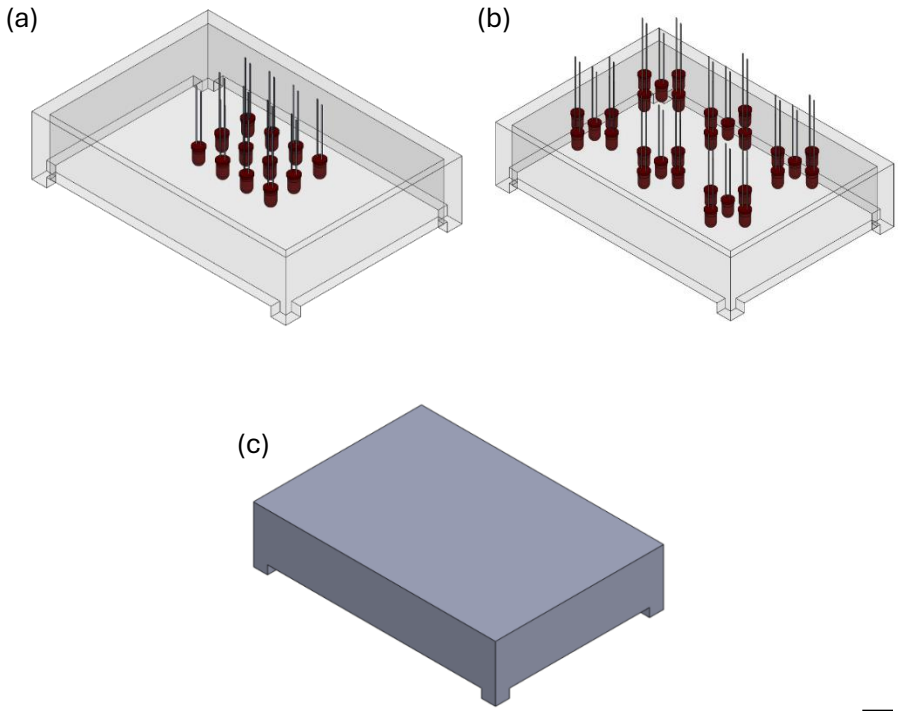

Figure 2: SolidWorks renderings of the custom designed 3D printable well plate covers for in vitro NIR photobiomodulation treatment. (a) 48 well plate covers outfitted with twelve 810 nm LEDs for twelve wells of treatment. This configuration of LEDs was chosen as the diameter of the LED is approximately equivalent to the diameter of the well diameter. (b) 6 well plate covers outfitted with thirty 810 nm LEDs. LEDs are in groups of five per well for all six wells. This configuration was chosen as it was the most even distribution with the least number of LEDs used that accommodated the diameter of the well. Covers for LED covers were printed from transparent PLA on a Prusa MK3S+. Transparent PLA was chosen due to its innate ability to scatter light. By scattering light with these covers it allows for the maximum exposure to be achieved. (c) Control plate covers were designed off the same dimensions as the treatment plate covers without holes for LEDs. Having control plate covers was necessary as it allowed the plate sets to be treated simultaneously outside of the incubator thus keeping test conditions consistent throughout all groups. Control plates were printed from black PLA on a Prusa MK3S+. Black PLA was chosen as black is a natural light absorber. By shielding the control plates in a light absorbing color material, we were able to assure that the control plates were not receiving any light exposure during the treatment period. Scale bar: 10 mm.

2.3 Experimentation

In vitro experiments were conducted on passage 3 (P3) frozen stocks of human mesenchymal stem cells (hMSCs) (Lonza, USA). Cells were recovered and allowed to reach 80%

confluency in growth media (DMEM high glucose GLUTAMAX (Gibco), 10% Fetal Bovine Serum (Gibco), 1% antibiotic-antimycotic (Gibco), 1% Non-Essential Amino Acids (Gibco), and 5 ng/mL basic fibroblast growth factor (Gibco)). After recovery and expansion, hMSCs were seeded in either six well plates, for qPCR, Elisa, and Western Blotting, or 48-well plates, for staining and Elisa, at a seeding density of 96,000 cells/well and 10,000 cells/well respectively. Two days post seeding, half of the experimental plates were shifted to osteogenic media (DMEM high glucose GLUTAMAX (Gibco), 10% Fetal Bovine Serum (Gibco), 1% antibiotic-antimycotic (Gibco), 100 nM dexamethasone (Sigma-Aldrich), 10 mM sodium β-glycerophosphate (Sigma-Aldrich), and 0.05 mM 1-ascorbic acid) to begin the initial differentiation, while the other half remained on a growth media regiment. Media was changed every 2-3 days for the duration of the study[27].

2.3.1 In vitro Light Treatment

Experiments were performed on groups of 4 plates, 2 control plates and 2 treatment plates, at a single time. Control plates were covered with solid black plate covers and treatment plates were covered with LED well plate covers. Plates were treated outside of the incubator for 10 minutes daily in a darkened room. Ten minutes was chosen as an initial exposure time to mirror the methods of Peng et al[7]. Prior to the first treatment, media was collected during the media change and froze for future assessment (Bone Morphogenic Protein 2 (BMP2) Elisa). In addition to the pre-collection, media was collected at every media change post treatment for the duration of the study. At 7, 14, 21, and 28 days a control and treatment plate were collected and processed for Live/Dead staining, qPCR, Western Blotting, and Phospho-SMAD staining.

2.4 In vitro Methods

2.4.1 Live/Dead Staining

Live/Dead analysis was performed at 7, 14, 21, and 28 days using an Invitrogen Live/Dead Cell Imaging Kit (Fisher Scientific). Kit components were mixed in the dark according to manufactures instruction and diluted in DMEM (Gibco). Media was aspirated from the wells and 0.5 mL of Live/Dead in DMEM was added to each well and incubated at 37ºC and 5% CO_2 for 30 minutes. After incubation, the media was aspirated and replaced with DMEM. Plates were wrapped in tinfoil to prevent light exposure until imaging. Plates were imaged using a BZ-X series Fluorescence Microscope (Keyence, Itasca, IL). Quantification of live/dead staining was done using ImageJ (NIH, Bethesda, MD) and the live/dead quantification add on.

2.4.2 Bone Morphogenic Protein 2 (BMP2) ELISA

At the end of the study, each media change point (~11 points, minimum 24 samples and maximum 96 samples per point) was thawed and processed to assess BMP2 levels using a R&D Systems Human BMP-2 DuoSet ELISA kit (Fisher Scientific) according to the manufacturer's instructions. Plates were read using a Varioskan LUX Multimode Microplate Reader (Thermofisher Scientific, Waltham, MA).

2.4.3 Cryptochrome 1 (CRY1) & Bone morphogenic protein 2 (BMP2) Western Blotting

Western blots were performed at 7, 14, 21, and 28 days to detect cryptochrome 1 (CRY1) and BMP-2 levels of the treatment and control groups. Media was collected and samples were washed 2 times with cold Dulbecco's Phosphate-Buffered Saline (DPBS). DPBS was aspirated and 100 µL of chilled lysing buffer (1 mL RIPA 10X Lysis Buffer (Millipore Sigma), 9 mL distilled water (Invitrogen), and 1 Pierce Protease and Phosphatase Inhibitor (Thermo Scientific)) were added to each well. A fresh buffer solution was prepared before each timepoint. Wells were scraped using a cell scraper, collected, and kept on ice for 30 minutes with occasional agitation. After 30

minutes, samples were centrifuged at 4ºC and 15,000 RCF for 15 minutes. Supernatant was collected and the pellets were discarded. Samples were kept on ice and moved to a -80ºC freezer for long-term storage.

Samples were placed on ice, allowed to thaw slowly, and prepared with 33 µL of SDS (~ 100 µL sample to 33 µL SDS). The positive control (CRY1 recombinant protein) was thawed and prepared using 10 µL recombinant protein, 90 µL UltraPure DNase/RNase-Free Distilled Water (Invitrogen), and 30 µL SDS. Samples and control were heated at 95ºC for 5 mins prior to gel loading. Ladder (5 µL), samples (30 µL), and positive control (5 µL) were loaded on a Blot 8%, Bis-Tris Plus WedgeWell Gel (Invitrogen) and ran in MES-SDS running buffer (Invitrogen) on a Mini Gel Tank (Invitrogen) at 200 V for 45 minutes. After 45 minutes, gels were removed, and proteins were transferred using a mini nitrocellulose iBlot 2 Transfer Stack (Invitrogen) on an iBlot 2 Gel Transfer Device (Invitrogen) at 20 V for 6 minutes. After transfer, the membranes were removed and trimmed in deionized water. Membranes were placed in 5% BSA and agitated for 1 hour at room temperature. After 1 hour, the 5% BSA was removed and replaced with either diluted (1:2500) CRY1 polyclonal antibody or diluted (1:2000) BMP2 monoclonal antibody and agitated at 4ºC overnight. The primary antibody was removed, and the membranes were washed 3 times in a solution of tris buffered saline and tween 20 (TBST) with agitation for 5 minutes. After washing, diluted secondary antibody was added and agitated for 1 hour at room temperature. The secondary antibody solution was removed, and the membranes were washed with TBST 3 times with agitation for 5 minutes. Chemiluminescent substrate was prepared according to manufacturer's instruction and added to the membranes for a 1-minute incubation. Membranes were then analyzed using a ChemiDoc Imaging System (Bio-Rad, Hercules, CA).

2.4.4 qPCR

qPCR was performed at 7, 14, 21, and 28 days for the following primers, GapDH, Runx2, Osteopontin (OP), bone sialoprotein (BSP), and BMP2 using an RNeasy mini kit (Qiagen). Samples were collected by first aspirating the media from each well followed by the addition of 350 µL of β-ME Buffer RLT (containing 10 µL of β-ME per 1 mL of Buffer RLT). The wells were scraped and transferred into 2 mL tubes, which were stored at -80°C. For RNA isolation, samples were thawed and pipetted up and down to ensure thorough mixing. Next the samples were transferred to Qiashredder tubes, and centrifuge at ~17,000 g for 2 minutes. Afterward centrifugation, the top portion of the tube was removed and discarded and 350 µL of 70% ethanol was added to each sample. The samples were then transferred into a spin column and centrifuged at ~17,000 g for 15 seconds. The flow-through was discarded and 700 µL of Buffer RW1 was added to the spin column and centrifuged at ~17,000 g for 15 seconds, followed by discarding the flow-through. This step was repeated with the addition of 500 µL of Buffer RPE. Then, an additional 500 µL of Buffer RPE was added and centrifuged at ~17,000 g for 2 minutes. The spin column was then placed into a new 2 mL collection tube and centrifuge at ~17,000 g for 1 minute. Transfer the spin column to a new 1.5 mL collection tube and 35 µL of RNase-free water was added directly onto the column membrane and centrifuged at ~17,000 g for 1 minute. Samples were kept on ice while their purity and quantity were assessed using a NanoDrop (Thermo Scientific, Waltham, MA). The ideal usable readout is above 1.75 for 260/280 and 260/230. Samples were stored at -80°C.

For cDNA synthesis, a High-Capacity cDNA Reverse Transcription kit (Applied Biosystems) was used. First, kit components and samples were thawed on ice and the necessary volumes for the master mix based on the NanoDrop results were calculated. Ideally, 1 µg of RNA should be used to synthesize 1 µg of cDNA. The master mix was mixed and 10 µL was transferred

into each tube followed by 10 µL of sample in water. Tubes were sealed and placed on ice prior to thermocycling. A MJ Research PTC-200 Thermal Cycler (Bio-Rad, Hercules, CA) with a pre-programmed cycle was used.

For qPCR, a 96-well plate was prepared by adding 10 µL of PowerUp™ SYBR™ Green Master Mix for qPCR (Applied Biosystems) to each well, followed by 8 µL of diluted cDNA and 2 µL of predetermined primers per well. The plate was sealed and centrifuged to collect the samples at the bottom and remove any bubbles. Plates were read using a Bio-Rad CFX96 Touch Real-time PCR Detection System (Bio-Rad, Hercules, CA) and a preprogrammed cycle.

2.4.5 Phospho-SMAD staining

Phospho-SMAD staining was performed at 7, 14, 21, and 28 days in accordance with the following protocol. Adherent cell cultures were aspirated and fixed with 200 µL of 4% paraformaldehyde (PFA) for 30 minutes. After which PFA was removed, and samples were washed 3 times with 500 µL of 1X Dulbecco's Phosphate-Buffered Saline (DPBS) (Gibco). Samples were then permeabilized by the addition of 400 µL of 0.1% Triton X-100 in DPBS for 15 minutes at room temperature. After 15 minutes, samples were washed 3 times in 500 µL of DPBS. Next samples were blocked with 2% bovine serum albumin (BSA) in DPBS for 1 hour at room temperature. Aspirated blocking agent was replaced with 500 µL of diluted primary antibody and incubated overnight at 4ºC. Primary antibody was aspirated and washed 3 times with DPBS followed by the addition of 500 µL of secondary antibody for 45 minutes at room temperature shielded from light. Lastly, secondaries were aspirated and washed 3 times with DPBS. An additional 500 µL of DPBS was added followed by sample imaging with a BZ-X series Fluorescence Microscope (Keyence, Itasca, IL).

2.5 Results & Discussion

Preliminary Live/Dead staining (Figure 3) of the control and treatment groups over a 15-day period showed that exposure to 810 nm light did not have a visibly significant impact on cell viability. To further confirm this and see if this held true over a longer experimental period, a follow up 28-day study was conducted. The results of the 28-day study (Figure 4) showed no visibly significant cell death in the treatment groups compared to the control groups. Further quantification of the Live/Dead images was performed using ImageJ (NIH, Bethesda, MD) and the accompanying live/dead quantification plug-in. Quantification values calculated in ImageJ for each day and for the control and treatment groups. Each data group consisted of three samples. Samples were averaged and plotted (Figure 5) with error bars equivalent to the standard deviation. Statistical analysis in the form of t-tests were conducted and showed no statistical significance present between the percent living cells of the control group (blue) and the treatment group (orange). These results are ideal as we do not want to have a significant difference present as that would be indicative of our treatment inducing harm to the cells.

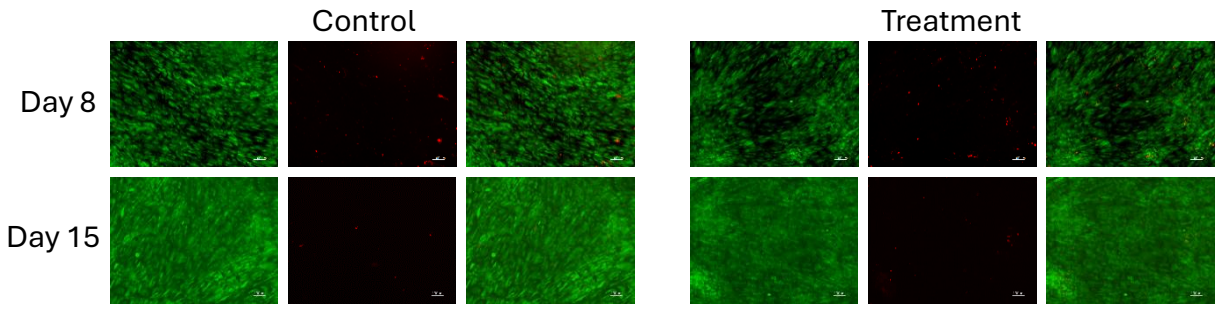

Figure 3: Preliminary study Live/Dead staining of control and treatment groups for days 8 and 15. The control group received no light therapy, and the treatment group received 10 minutes of 810 nm LED light each day. Live cells are shown in green (left column), dead cells are shown in red (middle column), and a merge image is shown in the right column. Images were taken with BZ-X series fluorescent microscope. Treatment does not show a visible negative impact on cell viability. Scale bar: 100 microns

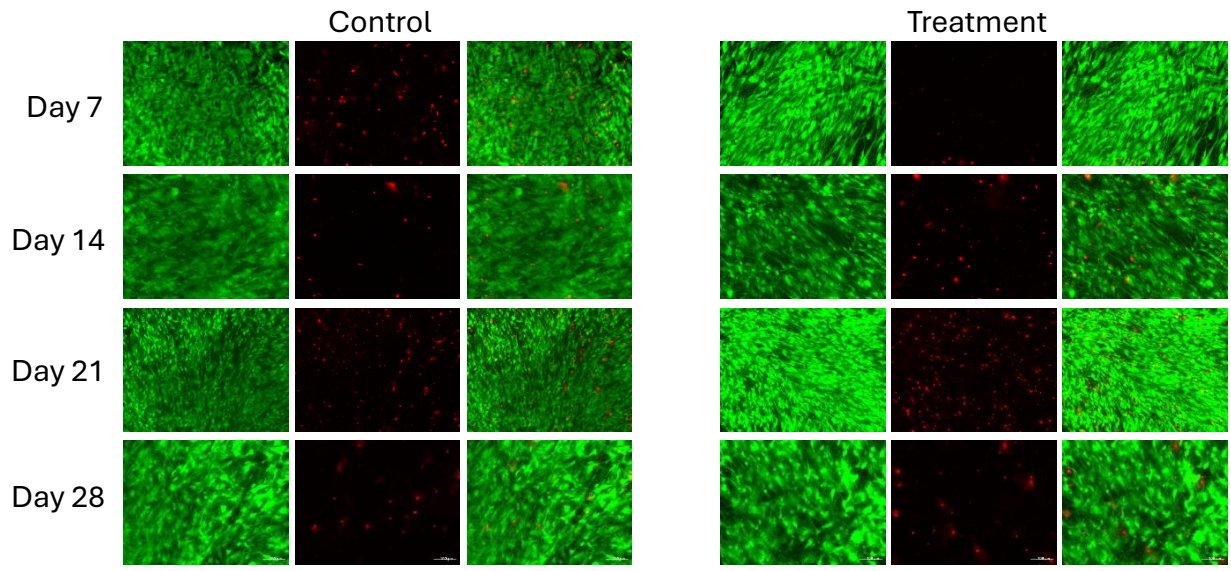

Figure 4: Live/Dead staining of control and treatment groups over a 28-day study. The control group received no light therapy, and the treatment group received 10 minutes of 810 nm LED light each day. Live cells are shown in green (left column), dead cells are shown in red (middle column), and a merge image is shown in the right column. Images were taken with BZ-X series fluorescent microscope. Treatment does not show a visible negative impact on cell viability. Scale bar: 100 microns.

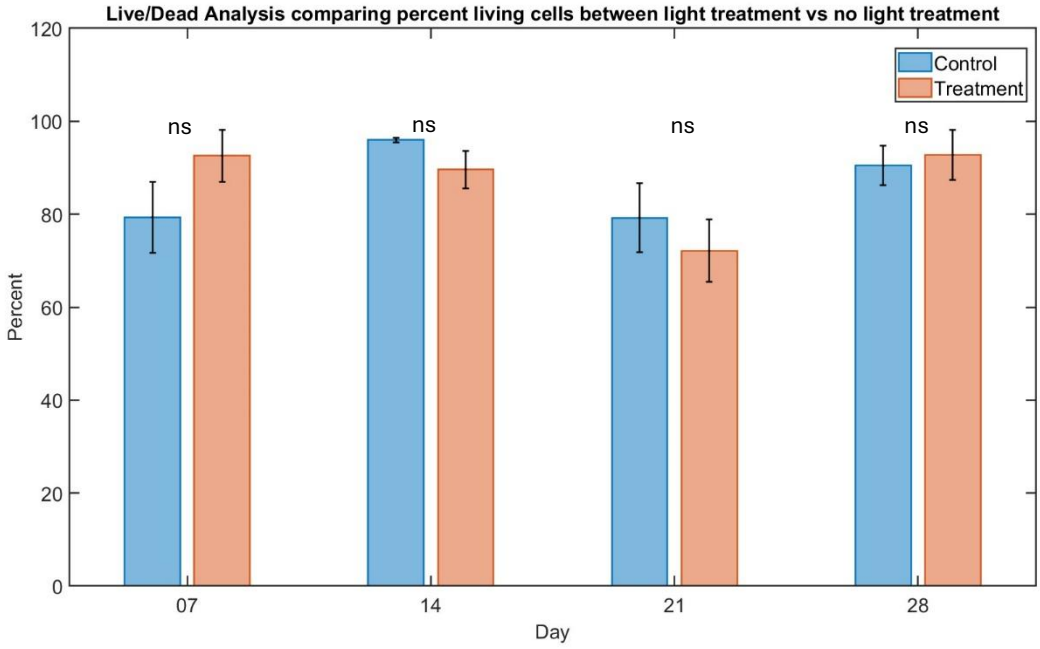

Figure 5: Quantification of the Live/Dead staining for days 7, 14, 21, and 28 for the control (blue) and treatment (orange) groups. Each bar represents an average of 3 wells and error bars are the standard deviation. A t-test was used to determine significance. No significance is seen between the control and treatment group for all time points.

Figure 6 shows the results of the BMP2 Elisa analysis across the 15-day preliminary experiment. Each group's data consisted of three samples. Samples were averaged and standard deviation was calculated for the error bars. Data was assessed cumulatively and statistical analysis in the form of t-tests were performed. The results in Figure 6 showed a positive trend with the treatment group showing a steady increase in BMP2 production overtime, which would be indicative of a positive trend relating to the regenerative process. Unfortunately, the preliminary data did not show any statistical significance. To build upon the preliminary results, an expanded, sample size and duration, study was conducted. Figure 7 shows the results of the BMP2 Elisa analysis across this 28-day experiment. Each group's data consisted of twelve samples. Samples were averaged and standard deviation was calculated. Data was assessed cumulatively and statistical analysis in the form of t-tests were performed. The results show a visible positive trend similar to what was seen in the preliminary data set; however, statistical significance was not observed.

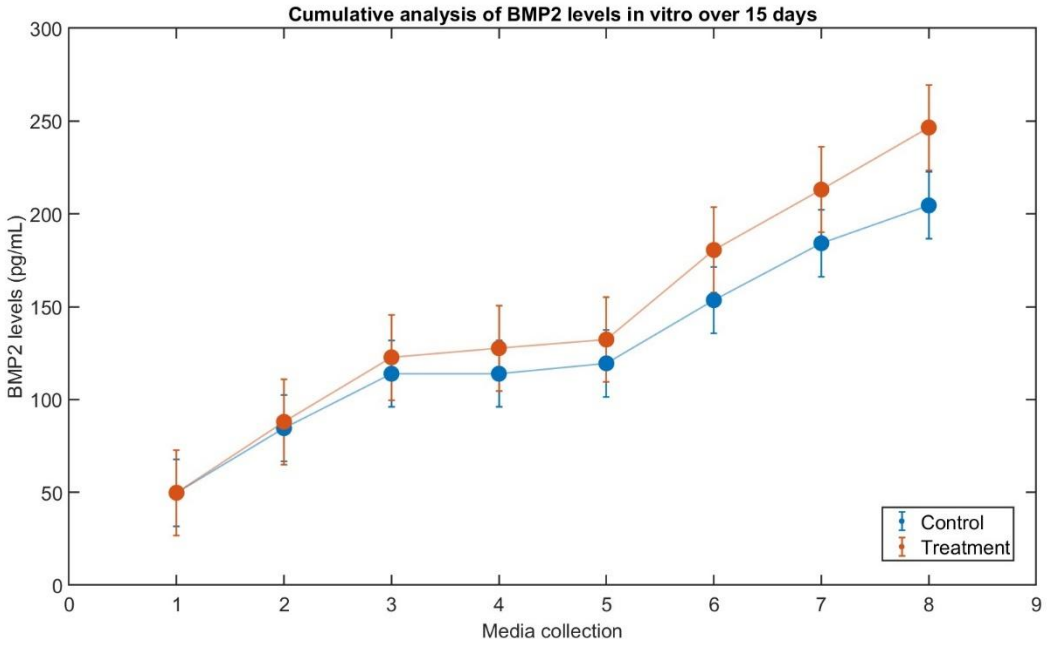

Figure 6: Preliminary cumulative ELISA analysis of BMP2 levels across 15 days of experimentation comparing control (orange) and treatment (blue) groups. Each dot represents an average of 3 wells and error bars are the standard deviation. A t-test was used to determine significance, to which no significance was observed.

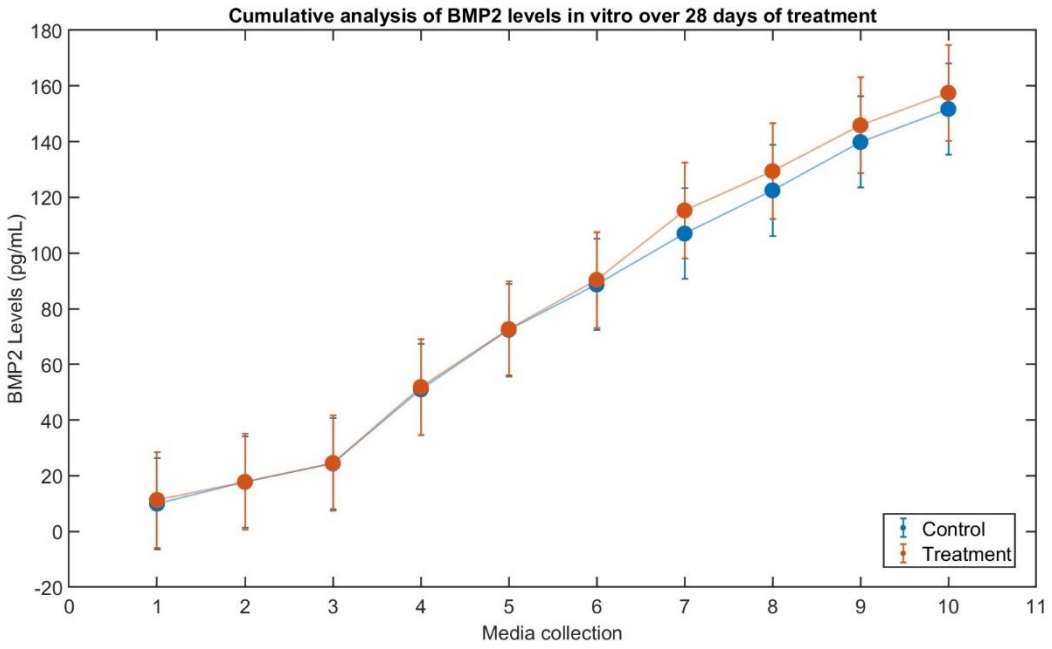

Figure 7: Cumulative ELISA analysis of BMP2 levels across 28 days of experimentation comparing control (orange) and treatment (blue) groups. Each dot represents an average of 12 wells and error bars are the standard deviation. A t-test was used to determine significance, to which no significance was observed.

Figure 8 shows the Western blot gel images of CRY1 for day 7 to day 28, where a visible decrease in band intensity (more whiteness) can be observed over the days. This decrease was confirmed using ImageJ to analyze each band's intensity (Figure 9). Six samples per group were averaged and the standard deviation was calculated. Statistical analysis was performed via t-tests. Gel analysis showed statistically significant changes in CRY1 levels between the control and treatment groups from day 14 to day 28. Figure 10 shows the preliminary western blot data for BMP2 analysis for days 7 and 14. There is a visible increase in band intensity between day 7 and day 14. Increased band intensity is indicative of increased levels of BMP2 protein in the gel. Further analysis with ImageJ was done to quantify the average intensities of the samples. Three samples per group were averaged and standard deviation was calculated, and are shown in Figure 11. Statistical analysis was performed via t-tests. Gel analysis showed statistically significant

changes in BMP2 levels for day 7 but not day 14. These results were interesting as it did not follow the anticipated trend seen in the CRY1 gel analysis. Figure 12 shows western blot gel results for the extended 28-day study. Increased band intensity is indicative of increased levels of BMP2 protein in the gel. Further analysis with ImageJ was done to quantify the average intensities of the samples. Three samples per group were averaged and standard deviation was calculated and are shown in Figure 13. Statistical analysis was performed via t-tests. Gel analysis showed that the growth media condition overtime showed significant increases in the levels of BMP2. However, for the osteogenic media condition, only day 7 showed significantly different levels of BMP2. A potential explanation for this could be because of the media itself, as this formulation of media's purpose is to push cells towards osteogenesis which results in secretions of BMP2.

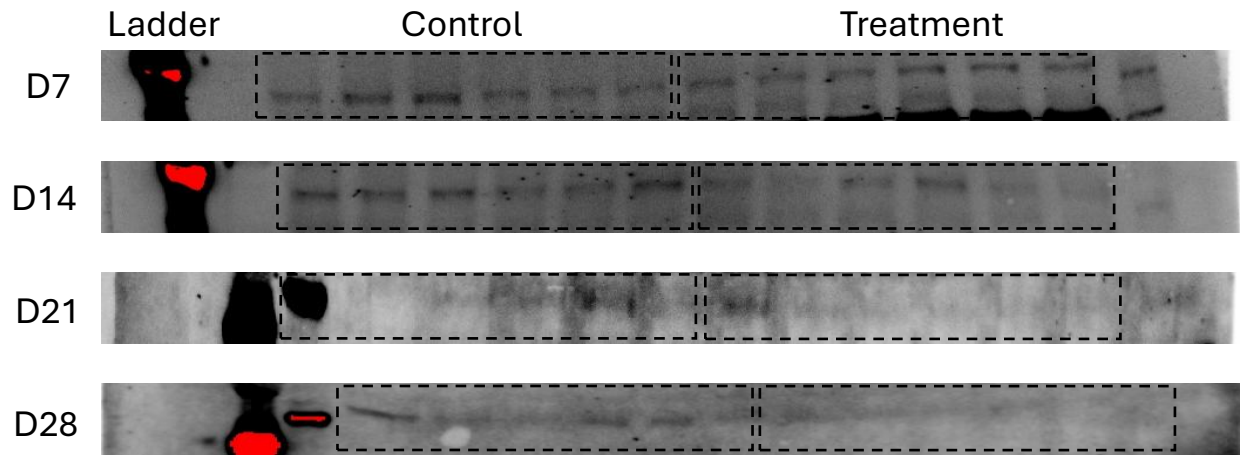

Figure 8: Western blot analysis of CRY1 protein levels of hMSCs over 28 days for control (lanes 3-8) and treatment (lanes 9-14) groups. A decreasing band intensity (whiter) is indicative of a drop in protein level. A visible decrease in the intensity is observable between the control and treatment groups. There is also an observed decrease over time for the same group. Gel images obtained using a Bio Rad ChemiDoc.

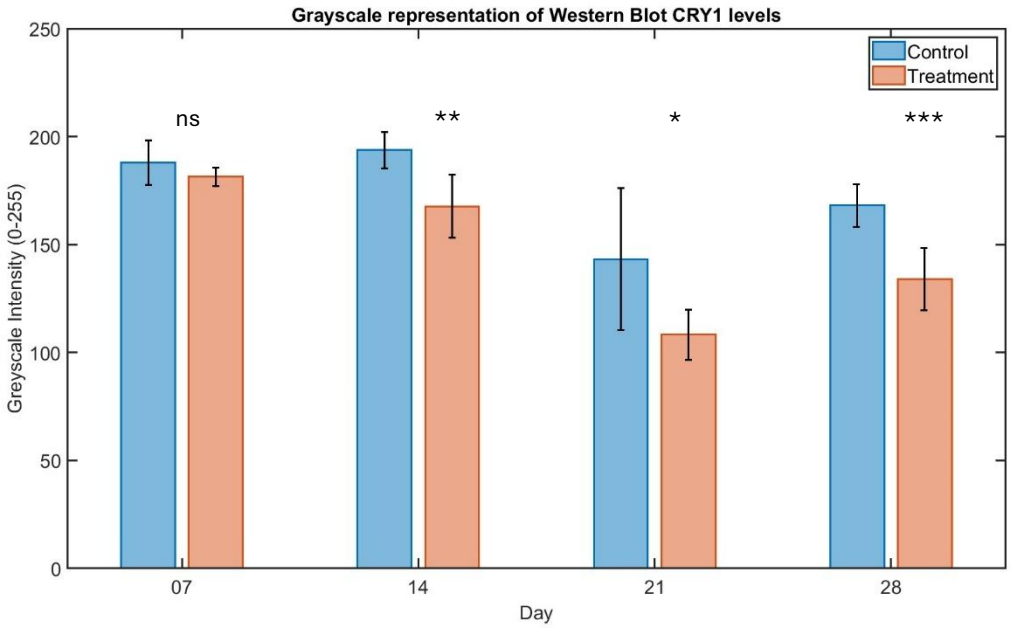

Figure 9: Quantification of CRY1 protein levels obtained from western blot numerically represented with grayscale intensity over 28 days. Western blot gel intensities were processed using ImageJ. Each bar represents an average of 6 samples and error bars are the standard deviation. T-tests were used to determine the level of significance. Y-axis scale represents intensity from 0-250 with 0 representing lowest levels of protein and 250 representing the highest levels of protein.

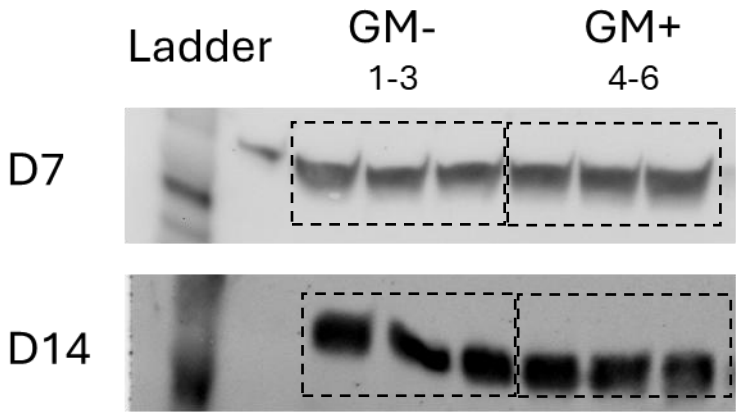

Figure 10: Preliminary western blot analysis of BMP2 levels of hMSCs over 14 days for control (lanes 3-5) and treatment (lanes 6-8) groups. Decreasing band intensity (whiter) is indicative of a drop in protein level. A visible shift in intensity is not observable from control to treatment group, however, it is visible overtime. Gel images obtained using a Bio Rad ChemiDoc.

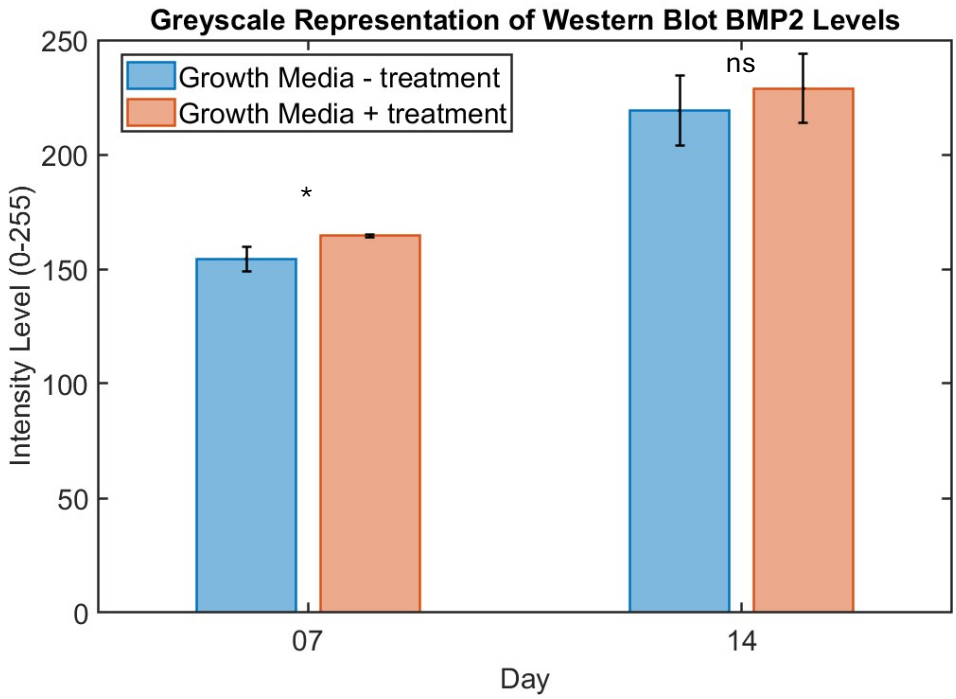

Figure 11: Preliminary quantification of BMP2 levels obtained from western blots were numerically represented with grayscale intensity values over 14 days. Western blot gel intensities were processed using ImageJ. Each bar represents an average of 3 samples and error bars are the standard deviation. T-tests were used to determine the level of significance. Y-axis scale represents intensity from 0-250 with 0 representing lowest levels of protein and 250 representing the highest levels of protein.

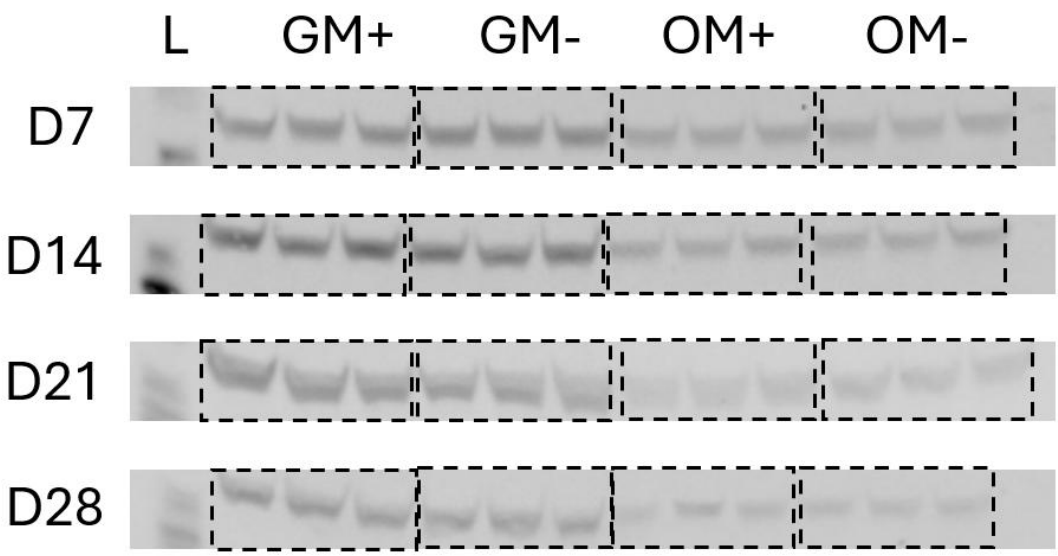

Figure 12: Western blot analysis of BMP2 levels of hMSCs over 28 days for growth media (GM) treatment (+) and control (-) and osteogenic media (OM) treatment (+) and control (-). Decreasing band intensity (whiter) is indicative of a drop in protein level. Gel images were obtained using a Bio Rad ChemiDoc.

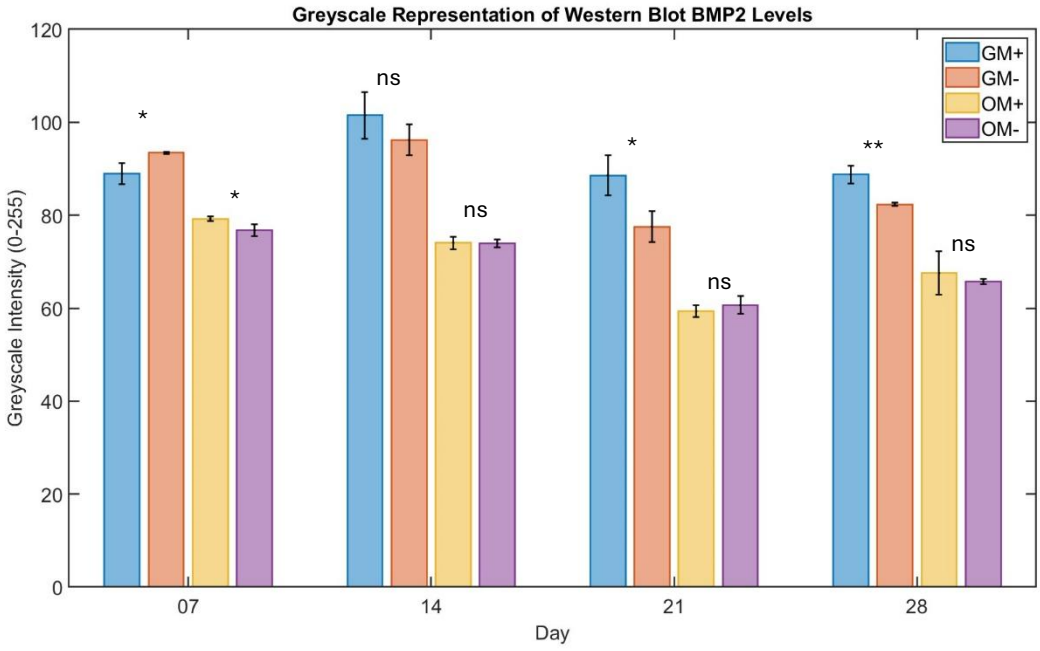

Figure 13: Quantification of BMP2 levels obtained from western blots were numerically represented with grayscale intensity values over 28 days. Western blot gel intensities were processed using ImageJ. Each bar represents an average of 3 samples and error bars are the standard deviation. T-tests were used to determine the level of significance. Y-axis scale represents intensity from 0-250 with 0 representing lowest levels of protein and 250 representing the highest levels of protein.

Figure 14 shows the initial qPCR fold changes in numerous osteogenic markers over a 28-day experiment for growth media with light treatment (GM+), growth media without light treatment (GM-), osteogenic media with light treatment (OM+), and osteogenic media without light treatment (OM-). All data is normalized to GM-, so all GM- bars are equal to one. Each bar on the graph represents three samples in triplicate. Standard deviation was used for the error bars. A fold change greater than or equal to 2 was considered a significant fold change as this meant that the observed gene was upregulated to two times that of the control. By day 28, Runx2 had steadily increased to an observably significant fold change. Unfortunately, processing of the osteogenic media samples was not reliable, which resulted in missing data points and unusual fold change values. Overall, the results observed indicated that our light treatment generated the output we

expected to see, decreased levels of CRY1 and increased levels of known osteogenic markers. These results are significant as it highlights the potential for this system to act as a future therapeutic for regeneration.

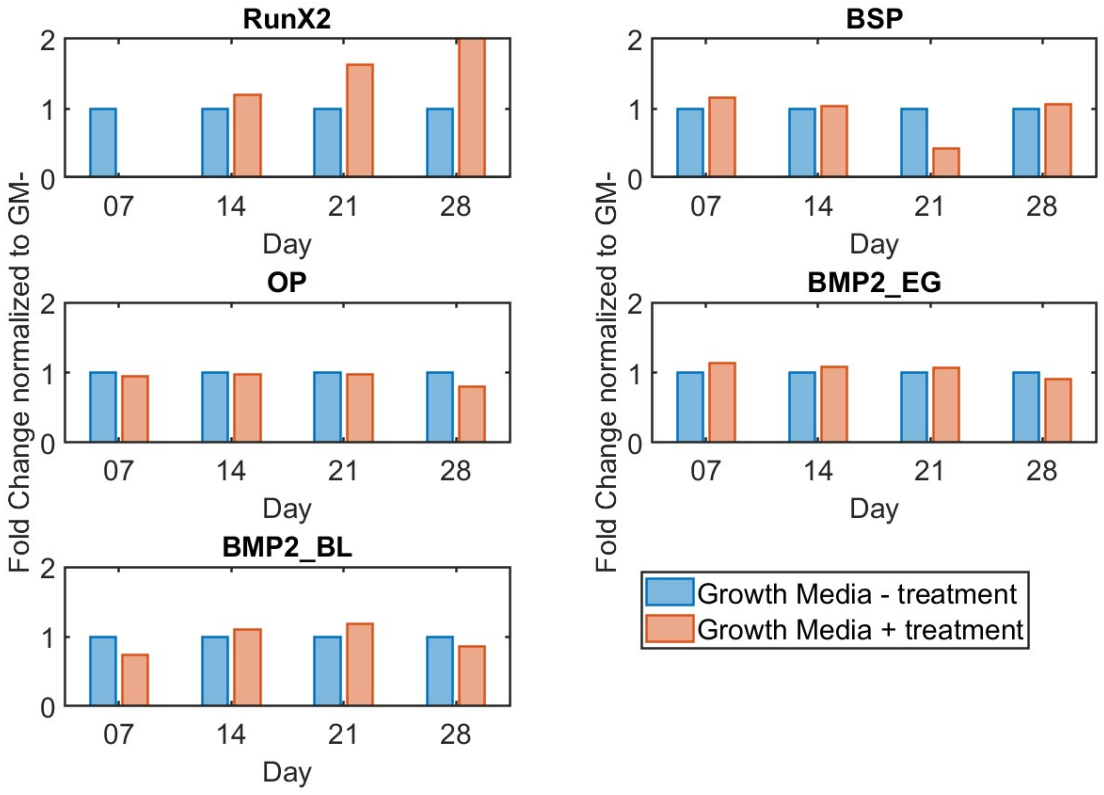

Figure 14:Preliminary relative qPCR for RunX2, BSP, OP, and BMP-2 over 28-days for control (blue) and treatment (orange) groups. All samples are calculating fold change relative to the control condition. A bar that is 2 or greater represents a two-fold change, which is deemed to be significant. Each bar represents an average of 3 samples run in triplicate and error bars are the standard deviation.

Unfortunately, phospho-SMAD staining did not produce any results as there was an unknown issue during staining. Potential issues could be related to the antibodies used to detect

and stain for phospho-SMAD. Due to time constraints, alternatives could not be tested and future work related to this project should explore these.

2.6 Simulations

Based on the results obtained from the in vitro studies, the feasibility of implementing this work in a mouse model was evaluated. Simulations based on a Monte Carlo model were run to generate an approximation of the light penetration depth with respect to power density (power per tissue volume) prior to device use with animal subjects. Simulations are meant to be representative of LED specifications and utilized a wavelength of 810 nm. Figure 15a represents the simulation of the hind paw within the complete device. The black half oval represents the cast and the back half circle represents the LED. The white space is representative of air and accounts for its optical properties. The point on the hind paw positioned closest to the LED receives the most power per tissue volume, and it begins to drop off from that location. Based on the simulation, an approximate length of 5 mm from the LED to the tip of the digit receives the highest amount of power from the LED. While up to 10 mm from the LED into the tissue still receives adequate but not optimal power. However, the power density at the deeper tissue further from the light source is lower and could potentially be out of the functional range of 1 – 1,000 mW/cm^2 [28]. Additional information is required to determine the power density at specific tissue volumes, such as source power and true tissue volume, to determine the functional range. To be consistent with the work of Peng et al. (2022), a power density of approximately 100 mW/cm^2 was targeted[7]. Figure 15b represents the simulation of the hind paw without the biodome sleeve, and shows a lower power density at deeper tissues compared to Figure 15a. This was included to highlight the additional optical properties provided by the cast, particularly the ability of the cast to direct photons toward the tissue, which aids in penetration depth.

Figure 16 shows the simulation of the hind paw using the external optical stimulation system. Figure 16a models the hind paw with respect to one LED, the position represented by "x", on the array and Figure 16b models the hind paw with respect to four LEDs on the array. The results of these simulations showed an order of magnitude drop in power per tissue volume compared to those of the internalized device (Figure 15). This is likely due to the design of the array, such as the LED spacing and the need for the photons to travel through air. As previously stated, additional information, including source power and true tissue volume, is needed to calculate the power density at a given tissue volume. This will be calculated using the diameter and length of the digit, of the mice with the LED's source power to determine the power density at specific depths in the tissue.

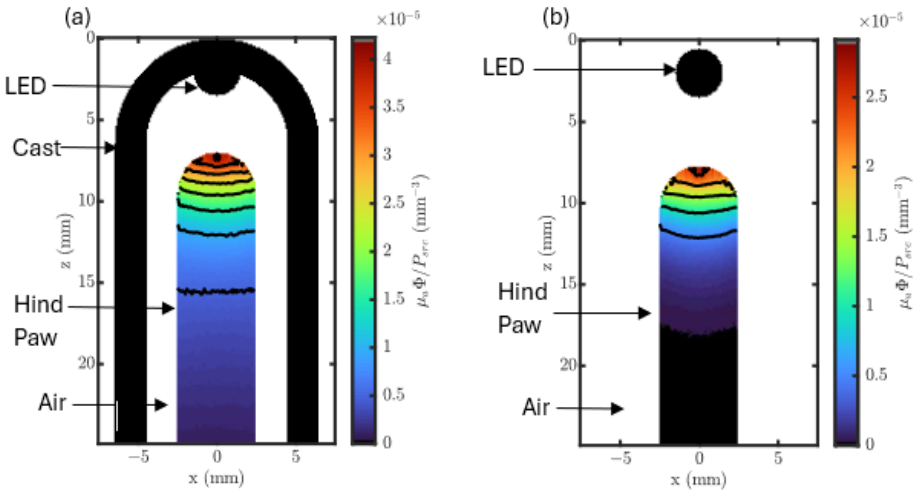

Figure 15: Monte Carlo simulations of the mouse hind paw with the LED (a) in the Biodome cast and (b) without the cast to compare the two scenarios. The black half oval represents the cast, the black circle represents the 810 nm diode position, and the white space represents air. The color gradient represents a transition in high to low power per tissue volume with red being the highest and blue being the lowest. Note the gradient scales are not the same in order to better visualize the drop in power present with the removal of the cast.

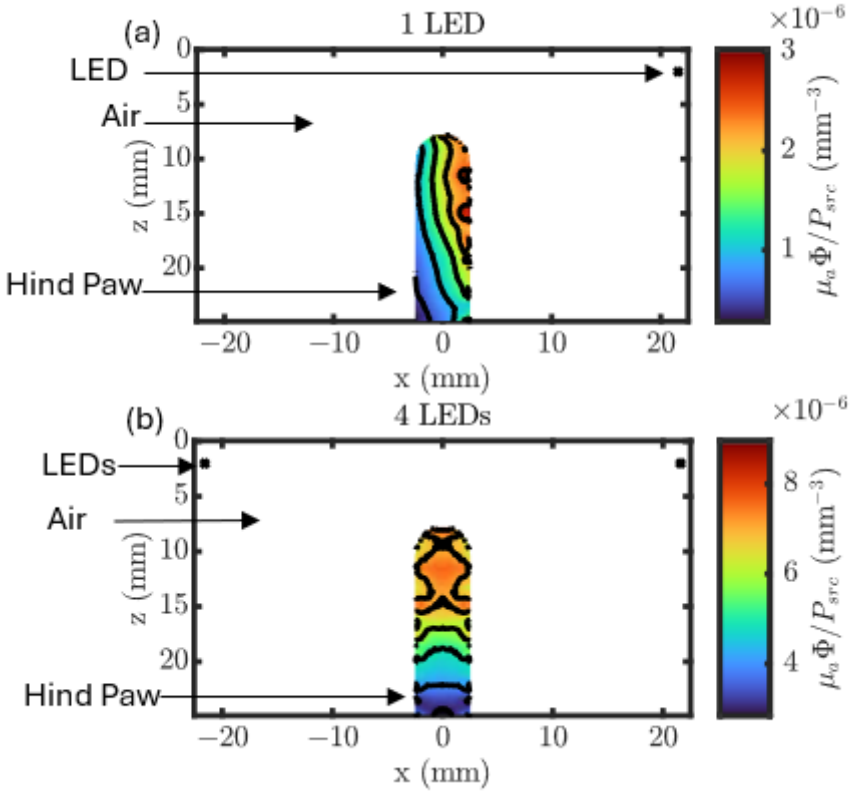

Figure 16: Monte Carlo simulation of the mouse hind paw using the externalized device for optical stimulation: (a) hind paw exposed to one 810 nm diode, (b) hind paw exposed to four 810 nm diodes, note only two are visible as the missing two would fall in a three dimensional plane. The "x" denotes diode position with respect to the hind paw. The color gradient represents a transition in high to low power per tissue volume with red being the highest and blue being the lowest.

2.7 Device Overview – in vivo

After promising steps were made with the in vitro studies, the next phase of in vivo work commenced. To be viable for in vivo studies, the devices had to undergo a redesign. Based on the results of the simulations, the design of an optical system that could fit within our preexisting cast was chosen. For this to be feasible, a number of specifications (Table 1) needed to be achieved. These specifications included the form factor, power, time scale, connectivity, and clarity. There was a total of 3 different form factors that were evaluated, which were a wireless internal LED, wired internal LED, and an external LED array. The internal wireless LED needed to be built into

the current biodome cast that is worn by animals in the secondary animal enclosure during testing and needed to be powered wirelessly via induction. The wired internal LED needed to be attached to a modified version of the biodome cast with epoxy and controlled by an external power supply and needed to allow animals to remain in their enclosure. The external LED array does not include a biodome cast, but instead needs to be an external platform that can support the animal's enclosure and can be powered by an external power supply. All 3 form factors need to supply light to the animal for 10 minutes continuously. A summarized view of all three form factors is shown in Table 3 and the component list required to build all 3 form factors are listed in Table 2.

Table 1: Design and specifications for in vivo studies

Design Feature	**Specific Metrics**	**Approach/Methods**
Form Factor		
Internal LED (wireless)	Biodome Cast: Length 19.75 mm, OD 9 mm Induction LED: Length 6.5 mm, OD 5.75 mm	Built into the current Biodome worn by the animal. Uses secondary animal enclosure during testing periods.
Internal laser diode (wired)	Biodome Cast: Length 19.75 mm, OD 9 mm Modified to accommodate optical fiber	Attached to modified biodome cast with epoxy. Controlled via external power supply. Allows animals to remain in home enclosure.
External LED Array	Polycarbonate base: ~34.3 cm L x 29.2 cm W (front) x 15.5 cm H LED (40x) OD: 5 mm LED Spacing: x-direction: 43 mm, 35.5 mm, 31.75 mm y-direction: 38 mm	External platform that can support the animal's enclosure.
Power		
Internal LED	Current: 350 mA Voltage: 3 V Power Density: 100 mW/cm^2	Wirelessly via induction
Internal laser diode (wired)	Current: 260 mA Voltage: 2 V Power Density: 100 mW/cm^2	Wired to external power supply.
External LED	Current: 100 mA Voltage: 1.55 V Power Density: 100 mW/cm^2	Wired to external programmable power supply. Wireless with respect to animal interaction.

Time Scale		
Internal (wireless/wired)	10 mins daily	Experiments conducted by hand (not automated)
External LED	10 mins daily	Experiments conducted by hand (not automated)
Connectivity		
Internal LED (wireless)	Wireless with respect to the animals.	Induction power.
Internal laser diode (wired)	Wired with respect to animals.	Externally powered and transmitted through an optical fiber.
External LED	Wireless with respect to the animals.	Externally wired power for LED array.
Clarity		
Internal (wireless/wired)	Housed in a clear biodome cast.	Basic photography capabilities
External LED	No cast present during experimentation	
Other metrics		
Internal LED (wireless)	Device Numbers: 20 initial 40 end goal	
Internal laser diode (wired)	Device Numbers: 1 initial More as needed	Caps threaded design allows for attachment for the treatment period and removal after.
External LED	Device Numbers: 5 initial More as needed	

Table 2: Component Breakdown

Components/Materials	Part Number	Vendor
Internal 810 nm diode	1214-SST-10-IRD-B90H-S810CT-ND	Digikey
808 nm laser diode	L808P200	Thorlabs
External 810 nm diode	1125-1158-ND	Digikey
Optical Fiber	M35L02	Thorlabs
Laser Diode Mount	LDM56	Thorlabs
Laser Diode Driver	505	Newport
Induction Coil	5141	Adafruit
24 V Power Supply	1528-5130-ND	Digikey
Programmable Power Supply	b09thwbhnv	Amazon
Polycarbonate Sheet	8574K43	McMaster Carr

Table 3: System Breakdown for the 3 different form factors for in vivo studies

System	Component	Requirements	Power Method	Animal Interface
Optics	Internal LED (wireless)	810 nm wavelength Current: 350 mA Voltage: 3 V OD: 4-6 mm Total Length: 4-6 mm 10 minutes daily	Induction	Built into Biodome cast worn by animal
	Internal laser diode (wired)	Diode: 810 nm wavelength Current: 260 mA Voltage: 2 V Fiber: OD: 3.18 mm Total Length: 4-6 mm 10 minutes daily	Laser Diode Driver	Optical fiber built into Biodome cast worn by animal
	External LED	810 nm wavelength Current: 100 mA Voltage: 1.55 V ~34.3 cm L x 29.2 cm W (front) x 15.5 cm H 10 minutes daily	External Power Supply	Platform

2.7.1 Internalized Device Fabrication

Two form factors for the internal device that utilizes the Biodome cast were listed in Table 3, with the differentiator being wireless and wired. The wireless form was developed first, as it allows animals to move freely. To conform to the specifications listed in Table 1 for wireless power, custom induction diodes were fabricated and an updated version of the Biodome casts were developed to accommodate them. The new cast was designed to be completely 3D printed, it consists of two threaded ankle clips and an accompanying threaded cap. Parts were printed from Formlabs Biomed Clear resin (Formlabs, Somerville, MA). Clear was chosen for its innate properties to scatter light, as it scatters light toward the digit from multiple angles which is ideal. All components were threaded post fabrication to allow for easy assembly between the ankle clips and the cap. The induction setup was fabricated using 2 large pre-built induction coil kits (Adafruit) and 810 nm surface mount LEDs (1214-SST-10-IRD-B90H-S810CT-ND, Digikey). The wireless

LEDs from the induction kit were removed from the coil using a hot air gun (Aoyue) and solder points were cleaned with solder wick. Fresh solder paste (SRA Soldering Products) was added to the solder points and the surface mount LEDs were soldered in place using the hot air gun. Functionality was confirmed using the other components of the kit. The newly outfitted LED coils were fixed into the base of the cast cover using a small amount of the Biomed Clear resin and UV cured for 2 hours. The design and fabrication process can be seen in Figure 17. Figure 18a-c shows an induction LED setup mounted into the newly designed cast. Figure 18d shows the treatment enclosure. Induction coils around the enclosure are powered from an external power supply to power the induction LEDs in the casts. After curing, diode functionality was confirmed again. Prior to animal attachment, devices were sterilized using isopropyl alcohol and functionality was confirmed.

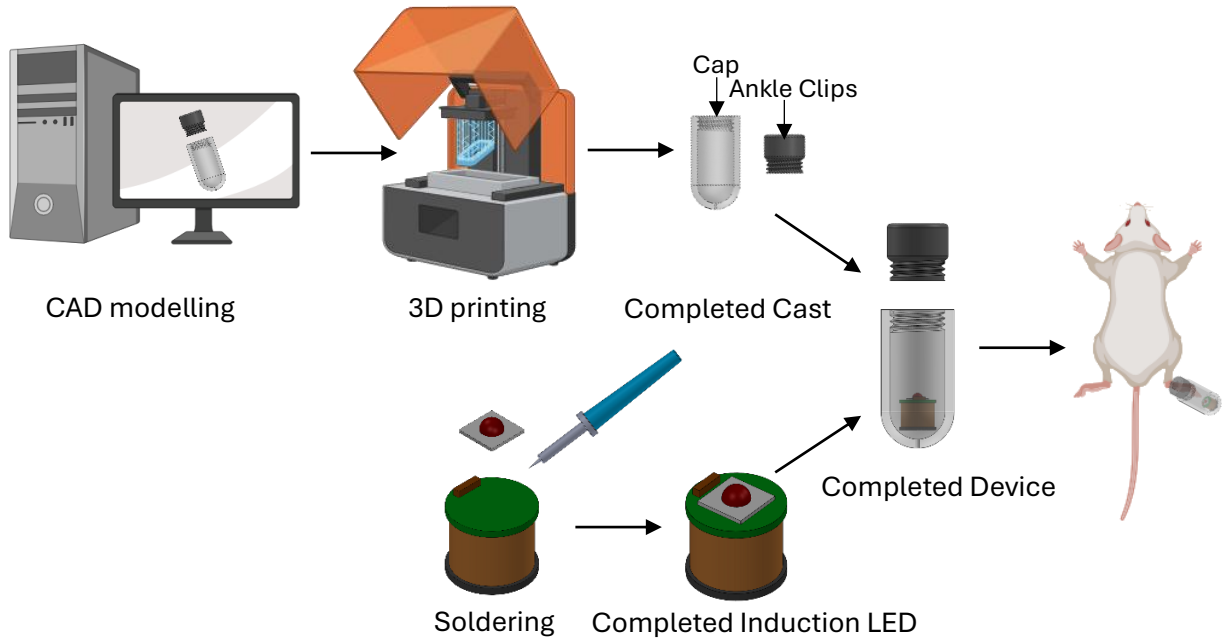

Figure 17: Process diagram for the wireless internalized device that includes CAD modeling and 3D printing of the cast, creation of the induction LED, and completed device.

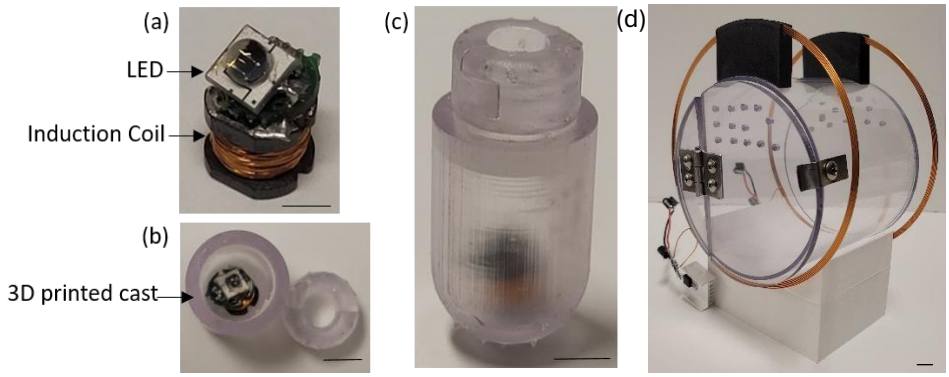

Figure 18: Internalized optical stimulation device and testing setup. (a) The 810 nm diode was soldered to a prebuilt induction coil before being fixed into position within the limb cast (b). A complete unit is shown in (c). The specialized testing enclosure (d) is used with the internalized optical device. Two induction coils are mounted horizontally to optimize power generation with respect to the positioning of the mouse hind paw. Scale bars: (a) 5 mm (b) 3.45 mm (c) 5mm (d) 12.7 mm

2.7.2 Externalized Device Fabrication

To prolong treatment up to 28 days after the initial 7 days of internalized treatment, an external device was designed. An initial concept of the proposed external device (side view) can be seen in Figure 19. Our goal for this device was to make use of the already existing mouse housing enclosures by constructing an array of LEDs that are arranged according to the enclosure's dimensions. The external treatment device was designed in SolidWorks as an array of forty 810 nm LEDs in the shape of the animals housing enclosure (Figure 20a). The device was fabricated from a 3.8 mm thick polycarbonate sheet (McMaster Carr). Through holes of 5 mm were drilled into the sheet 38.1 mm apart vertically and 35.6 mm apart horizontally for the LEDs (1125-1088-ND, Digikey) to be fit into. LEDs were secured in place with a dot of generic super glue. To power the array from one connection point, LEDs were wired together using solid core wires and a solder iron. LEDs were powered using a Hanmatek 305T power supply (1.80 V, 0.4A). Four legs were 3D printed from PLA using a Prusa MK3S+ to raise the array by 101.6 mm to prevent the array from crushing the wiring.

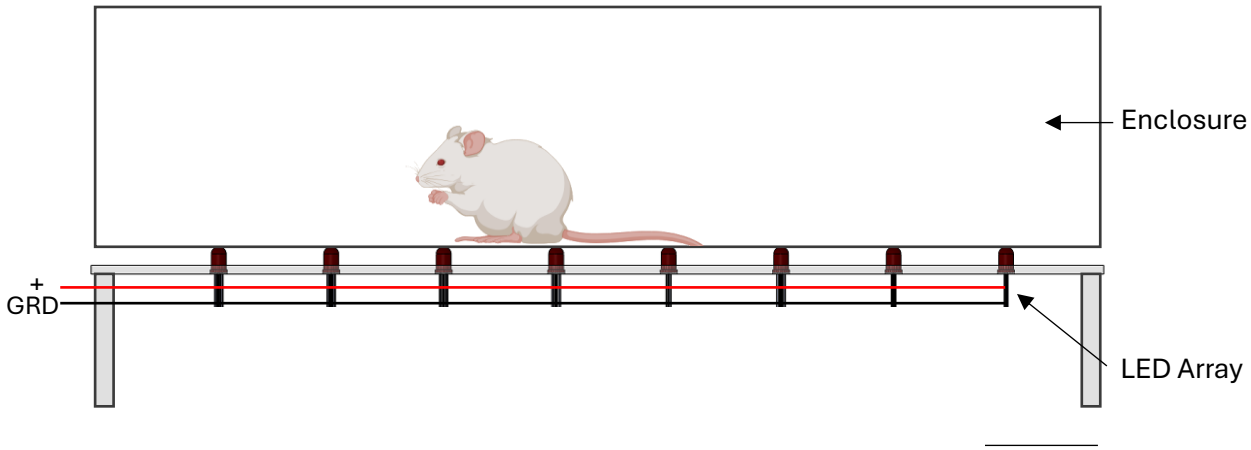

Figure 19: Concept design for the external optical array system. Initial designs were generated using SolidWorks and prototypes were fabricated out of a sheet of polycarbonate. The mouse enclosure with the mouse inside is placed onto pot the external optical array system. The array is held up by 4 legs and has a total of 40 LEDs that are evenly spaced throughout and can be seen in red. All LEDs were wired together so that all were powered on and off at the same time. Scalebar: 38.1 mm

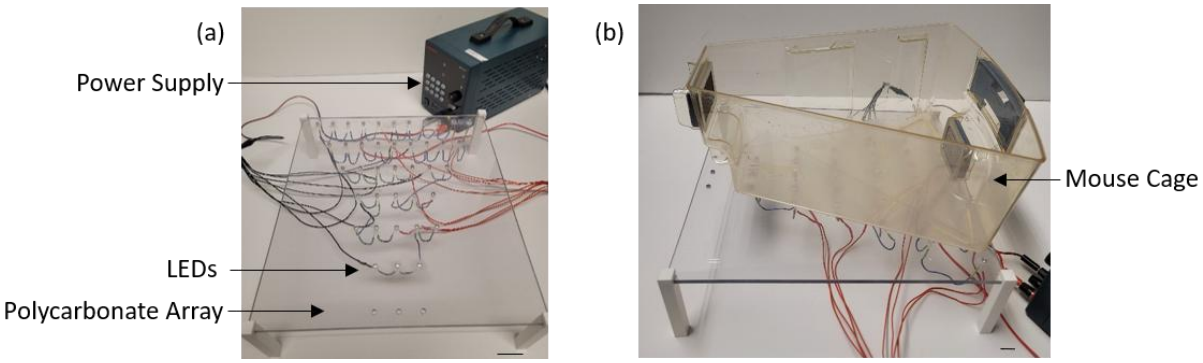

Figure 20: External optical stimulation setup without (a) and with (b) mouse enclosure. This system is designed for use after the cast has been removed to continue to provide optical stimulation to the amputation site. Array was fabricated from a polycarbonate sheet with through holes patterned to the shape and dimensions of the enclosure for the LEDs to be outfitted into. Scale Bars: (a) 43.2 mm (b) 12.7 mm

2.8 Experimentation

In vivo studies were conducted in a sterile surgical environment following the steps outlined in Figure 21 below. Figure 22 summarizes the entire experimentation process from start to finish.

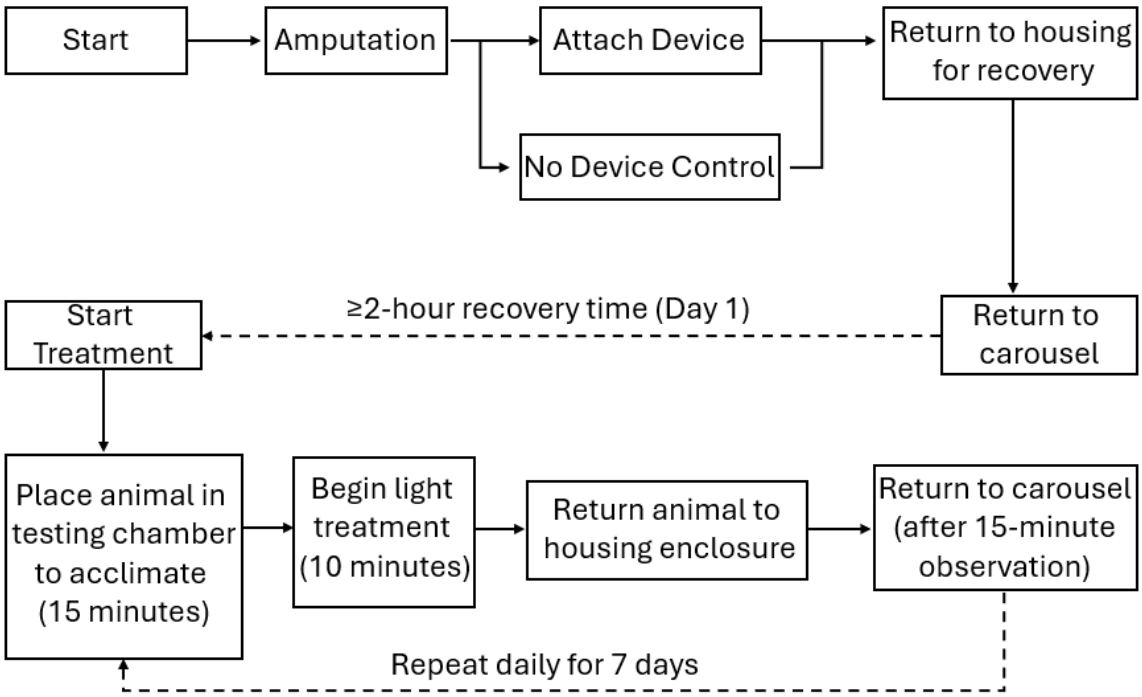

Figure 21: Flowchart of surgery and internalized treatment plan. Control group animals received no devices and were returned to their housing enclosures after bleeding had been reduced. Treatment group animals received their devices after bleeding was reduced. The animals were returned to their housing enclosure and placed back on the carousel in their temperature-controlled room. Surgery, device attachment, and the first treatment all occurred on the same day. A two-hour recovery period was added between device attachment and treatment for the animal's recovery and comfort. Treatment was conducted in a custom testing chamber that the animals were moved to and allowed to acclimate to for fifteen minutes. After acclimation, animals were treated for ten minutes. After treatment, animals were observed in their housing enclosures for fifteen minutes before being returned to the carousel.

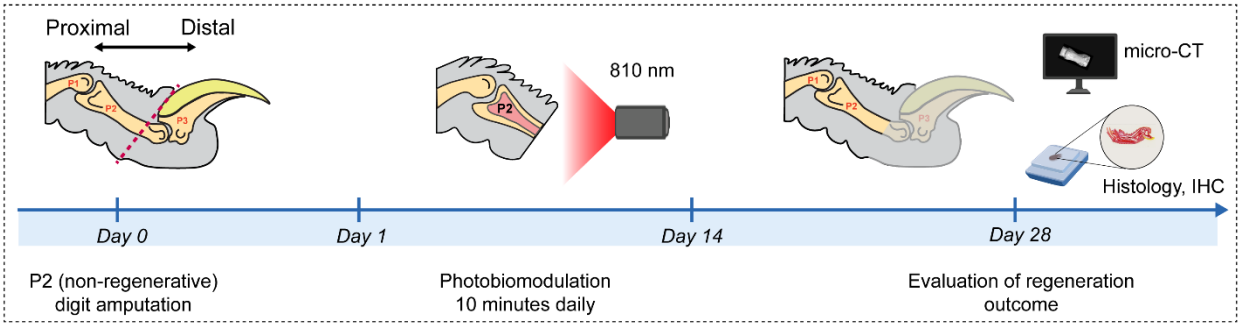

Figure 22: Summarized view of the surgical and treatment course for CD1 mice from day 0 to day 28. Sterile P2 amputation of the hind paw digit (red dashed line) occurs on day 0. Following digit amputation, animals were allowed to recover as outlined in the flow chart (Figure 21). At the end of the treatment period, animals are humanely sacrificed according to approved IACUC protocols and processed for evaluation via micro-CT and histology.

2.8.1 Internalized Device Attachment

Bleeding was minimized by applying mild pressure to the hind paw and the animal was allowed to wake up and return to its housing enclosure for ~ 1-2 hours. After bleeding was confirmed to have stopped, animals were anesthetized again, and the custom treatment devices were attached. Note this time gap was added to prevent blood accumulation in the device. The animals were allowed to wake up before being returned to their housing enclosures. For day 1 treatment, animals were allowed a maximum of 2 hours to acclimate to the cast prior to beginning the treatment. Treatment with the custom cast devices was performed for seven days in accordance with protocol M2022-128. Treatment was conducted in a custom-built cylindrical enclosure outfitted with large induction coils (Figure 18d). Treatment was administered for 10 minutes daily for the first 7 days. Figure 23a and Figure 23b shows a CD-1 mouse post amputation with an attached device. Figure 23c shows the same mouse in the testing chamber receiving treatment.

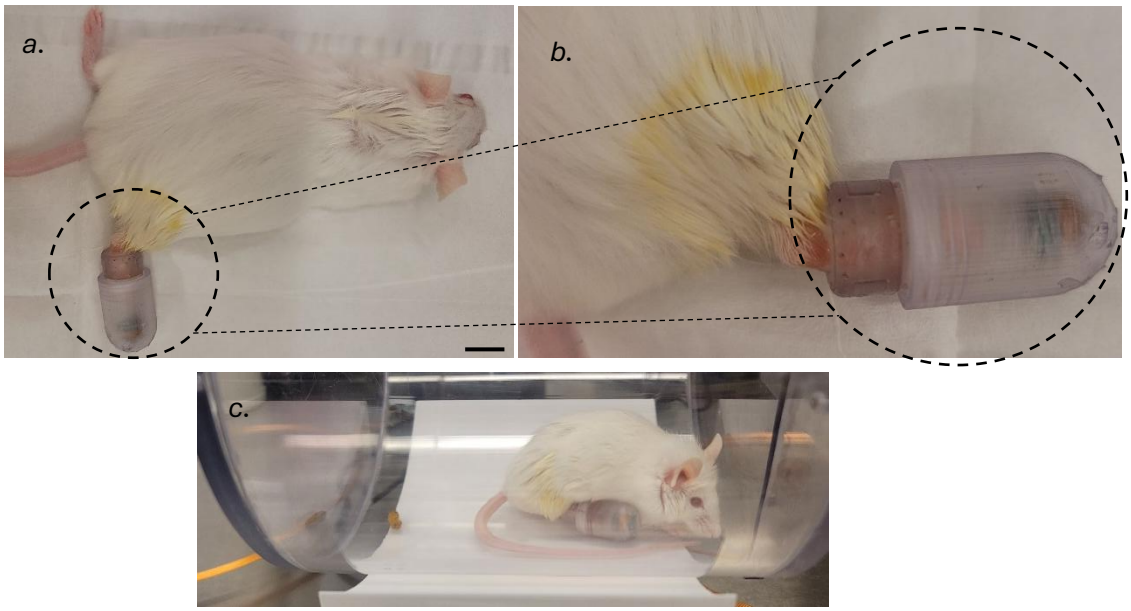

Figure 23: Initial in vivo study of internal optical stimulation system. (a.) Shows the updated device attached to the animal with a zoom in of the device (b.). (c.) Shows the animal with devices in the testing chamber receiving treatment. Scale bar: 10 mm.

2.8.2 Externalized Device Treatment

For continuation up to 28 days, the external device consisting of the LED array (Figure 20) was used. A fresh bedding free animal enclosure was placed on the device (Figure 20b). Animals were placed in the enclosure and allowed to acclimate for 15 minutes. Treatment was administered for 10 minutes daily over the remaining time of the study. After 28 days, animals were humanely sacrificed following previously established IACUC protocols and processed for data collection and analysis.

2.9 In vivo Methods

In vivo experiments were conducted on female CD-1 mice (Charles River Laboratories) using the custom treatment devices seen in Figure 18 and Figure 20.

2.9.1 Internalized Device Sterilization

Ethylene oxide and isopropyl alcohol sterilization methods were used for device sterilization prior to use. Ethylene oxide sterilization was performed using an Anprolene AN75i

(Andersen Sterilizers, Haw River, North Carolina) sterilizer. The sterilizers preprogrammed 12-hour cycle was used to sterilize devices. Electronics were sterilized with 70%, to remove microbes, and 99%, to remove any oils or leftover flux from soldering, isopropyl alcohol for 1 minute.

2.9.2 Limb Amputation

All surgeries were approved by Tufts University IACUC under protocol M2022-128. CD-1 mice were prepared for P2 amputation surgery using approved protocols. Surgery preparation, under anesthesia, for each animal was done with a combination of Betadine (Perdue) and alcohol swabs (BD) three times each. Control and treatment animals received P2 amputations of right hind paw middle digit under a microscope using a scalpel. Any bleeding was stopped with mild pressure applied to the digit and a cotton swab. Control animals were returned to their housing enclosure post bleeding reduction with no device. Treatment animals were returned to their housing enclosure post bleeding reduction with the internalized device. To prevent the possibility of animals removing the device prematurely, the ankle clips were secured in place with a dot of Skin Tite^{TM} (Smooth-on).

2.9.3 Histology and Immunostaining

Post treatment, animals were sacrificed humanely using standard IACUC approved protocols. The digits were harvested and fixed with 4% paraformaldehyde (PFA) at room temperature for 24 hours. Following PFA fixation, samples were removed and washed in 1x PBS four times. The samples were left in the last PBS wash overnight at 4ºC. PBS was replaced with fresh PBS for 10 mins followed by the addition of Surgipath decalcifier I for 2 hours. After 2 hours, the decalcifier was removed and replaced with fresh decalcifier and allowed to sit overnight. Tissues were then washed four times with PBS before undergoing graded ethanol dehydration. After treating overnight at 4ºC, 100% ethanol solution was replaced with xylene and placed under vacuum for 1.5 hours two times. Samples were then transferred into molten paraffin for infiltration.

This was done twice for 2.5 hours each under vacuum. Samples were then fully embedded in paraffin and sectioned using a microtome (Leica Biosystems, Nussloch, Germany)[6]. Following sectioning, samples underwent standard hematoxylin and eosin staining protocols.

2.10 Results and Discussion

In vivo experiments showed initial success with respect to device attachment and acceptance. These were accomplished with the modified design from the original biodome cast system to be a combination of an ankle clip and screw on cap. This modified design maintained the same ankle clip system that was used on the initial biodome cast by replacing the printed extension with a shorter threaded extension. The polypropylene cap was replaced with a long variant that was threaded to receive the updated ankle clips. Unlike the original, the design is wider; outer diameter of 13 mm compared to 10 mm and inner diameter of 9.75 mm compared to 7 mm. Upon observation with an animal subject, the cast was received similarly to the original design, which was taken positively as the animals accepting the modified systems. Though still requiring glue for additional support about the ankle, overall, the cast was both easy to attach and allowed for ease access to the wound site post-surgery as needed. The decreased amount of glue required for attachment provided additional comfort to the animals as excessive amounts of glue would get stuck in the fur causing irritation resulting in the animals gnawing the glue off.

Treatment was applied to animals over the course of 28 days. During that time, the first 7 days of treatment used the internal cast diode system. Unfortunately, the system relied heavily on animal positioning within the testing enclosure and due to animals' curiosity and movement resulted in very low exposure time, between 25%-32%. Table 4 shows a breakdown of each day of treatment and the exposure time each animal received. The remaining days of treatment switched from the internal system to the external array system. Due to the external systems setup,

animals received ~100% exposure to the light during treatment period. MicroCT of the digits (Figure 24) showed a decrease in the development of fibrosis in the treatment group compared to the control group. These initial results are promising as a decrease in fibrosis would be highly beneficial for the bone regeneration process as fibrosis scar tissue impedes further regeneration and can result in additional health issues. Histology of the digit showed potential re-vascularization of the amputation site (Figure 24). Re-vascularization would be incredibly beneficial to the regenerating limb as access to blood flow is critical to tissue health. These initial in vivo studies showed promising results for light treatment as an option to enhance the regenerative process non-invasively, however, these studies are still very preliminary and on a small sample set thus further experimentation is necessary to provide a significant assessment of the treatment.

Table 4: Percent internal device treatment exposure time per animal. Each treatment was recorded and an estimation of exposure time in seconds was collected. Exposure time was defined by the animal's relative position in the testing chamber as only certain orientations, coils in alignment, would result in activation of the induction system. Percent exposure time was calculated by dividing the estimation by the desired total time (10 minutes) then multiple by 100.

Exposure Time Estimations (seconds)			Percent Exposure Time (%)	
Treatment Day	M19	M20	M19	M20
1	229	311	38.2	52.2
2	238	82	39.7	13.7
3	108	319	18.3	53.7
4	202	35	33.9	5.8
5	130	173	21.8	29.1
6	63	300	10.6	50.0
7	92	97	15.3	16.2
Average Percent Exposure Time (%)			25.4	31.5

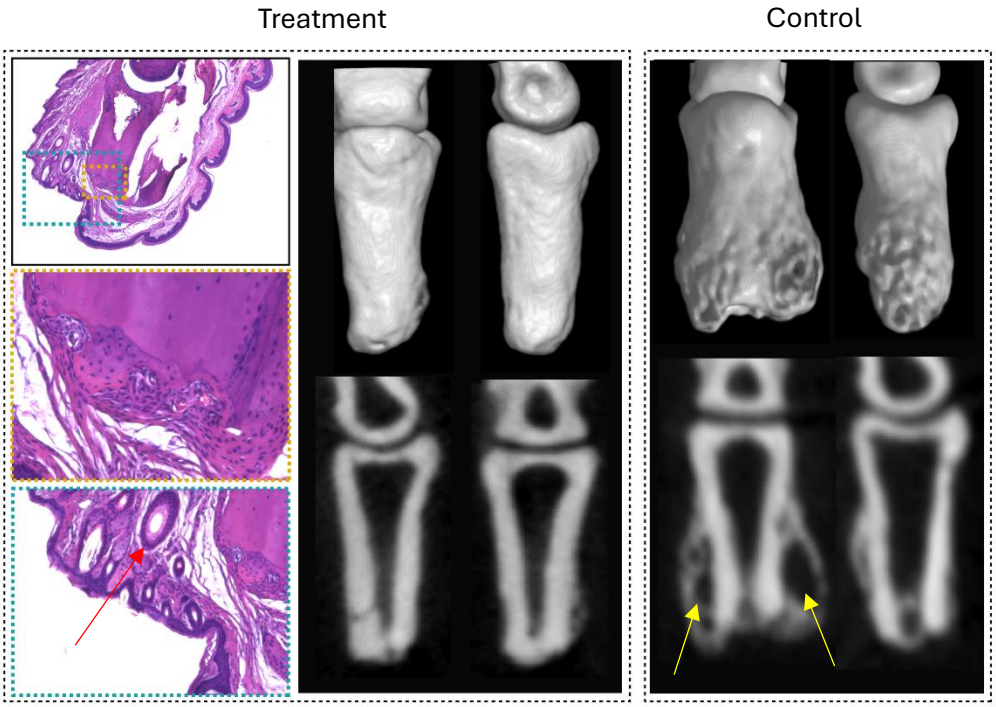

Figure 24: Histology and micro-CT images of mouse digits of treatment animals (left) and control animals (right). Histology images of treatment digit showed potential revascularization at the amputation site (red arrow). Micro-CT images showed a decrease in fibrosis in the treatment group verse the control group (yellow arrows).

2.11 Limitations

Limitations with the in vitro systems were minimal with the only notable one being the number of devices able to run at a given time. With only one power supply and two treatment covers, experiments became very time consuming. The major limitation in the optical stimulation was in the in vivo wearable device. Due to the induction system requiring precise positioning within the testing chamber, both animals were not able to receive the desired level of treatment exposure.

2.12 Conclusions

Devices were successfully designed and fabricated for both in vitro and in vivo optical stimulation. In vitro testing showed that our treatment was not inducing any negative impact on

overall cell health as well as showed preliminary success in the reduction of CRY1 and an increase in osteogenic markers. In vivo testing revealed issues with the internal devices that need to be addressed but overall showed initial promise as a treatment method showcasing a decrease in fibrotic tissue development and potential re-vascularization.

2.12.1 Future Directions

To build upon the initial in vitro work, exploration of alternative power densities outputs and there relation to treatment time should be explored to optimize treatment. With the ultimate goal of this work being implemented for human use, optimization for the shortest treatment time with maximum results is ideal. To build upon the in vivo work, the first component that needs to be addressed is the internal device. Induction proved to not be the best option for powering the devices as it requires very precise positioning within the testing chamber. Due to the devices small form factor powering can be difficult to achieve. Some alternative options to explore would be micro batteries as the main source of power. However, this would require a small microcontroller to control the devices powering on and off, which makes this option challenging. For larger patients, this method of device fabrication (control board with battery power) will be much easier to attain. Another alternative could be to transition from a wireless system to a wired system. A wired system would be ideal as it can be fabricated in a small form factor with more reliable light exposure to the digit. However, the implementation of the daily treatment would result in additional time as the wired system would not be able to be always attached to the animals in the housing room. Therefore, prior to treatment, a generic cap would need to be replaced with the wired treatment cap. With the updated threaded cap model used throughout this study, this variation of treatment will be easy to accommodate. Additionally, expanding both in vitro and in vivo studies to include multiple controls may be insightful to see if there are visible differences observed in healing and regeneration. Use of complete darkness controls, ambient light controls, and our

treatments may show different biological mechanism activation, which may have alternative effects of regeneration.

Chapter 3: Electric Field Stimulation for Regeneration

3.1 Introduction

Electrical signals are a prominent part of human anatomy and control many aspects of its functionality. In medicine, electrical treatments have been used to treat a number of different nervous system diseases, such as movement disorders or epilepsy[29]. These treatments include neuromodulation and neuroprostheses[29]. In addition to these, electrical stimulation has been used to heal skin wounds and regenerate nerves[12]. Previous work in rat amputation models showed that application of electrical stimulation at the amputation site resulted in new bone, cartilage, and vessel formation[12].

Electric fields (EF) are generated from charges, positive or negative[30]. These charges will either attract or repel from one another generating a force[30]. In the human body, as a response to injury, endogenous electric fields created by the movement of ions are generated to direct cells and modulate wound healing[31]. Previous work in the field of EF stimulation have shown that a field of up to 10 V/cm for up to 72 hours was capable of controlling cell orientation and migration without effecting cell viability[32]. While pulsed EFs have shown promise for osteogenic differentiation[32].

Manipulation of electric fields can therefore be a non-invasive form of electrical stimulation that can aid in numerous biological functions, such as regeneration and guided cell migration[11,12,32]. Use of electric field manipulation is ideal for our purposes as it is non-invasive and easily inclusive in the finalized proposed system.

3.2 Device Overview – in vitro

3.2.1 Design and Fabrication – in vitro

To provide a uniform and controlled EF, an initial prototype device was designed and fabricated. A custom 3D printed guide was fabricated to not only support copper plates needed to generate the EF but also maintain proper placement of well plates for repeatability and uniformity (Figure 25). The guide was printed out of Clear resin (Formlabs, Somerville, MA) on a Form 3B+ printer (Formlabs, Somerville, MA). The outer dimensions of the guide are 127 mm wide, 153.4 mm long, and 12.7 mm thick. An etch of 85.5 mm wide, 127.6 mm long, and 1.27 mm deep was placed centered to the bottom of the guide for the experimental well plate placement. Copper plates (McMaster Carr, Elmhurst, IL) were cut to the following specifications, 1127.5 mm long, 1.4 mm wide, and 50.8 mm tall. Each copper plate was then slotted into place on the guide's printed track 111.5 mm apart. Power to generate the field was applied to the cooper plates by a Hanmatek 305T power supply (Hanmatek, Shenzhen, China).

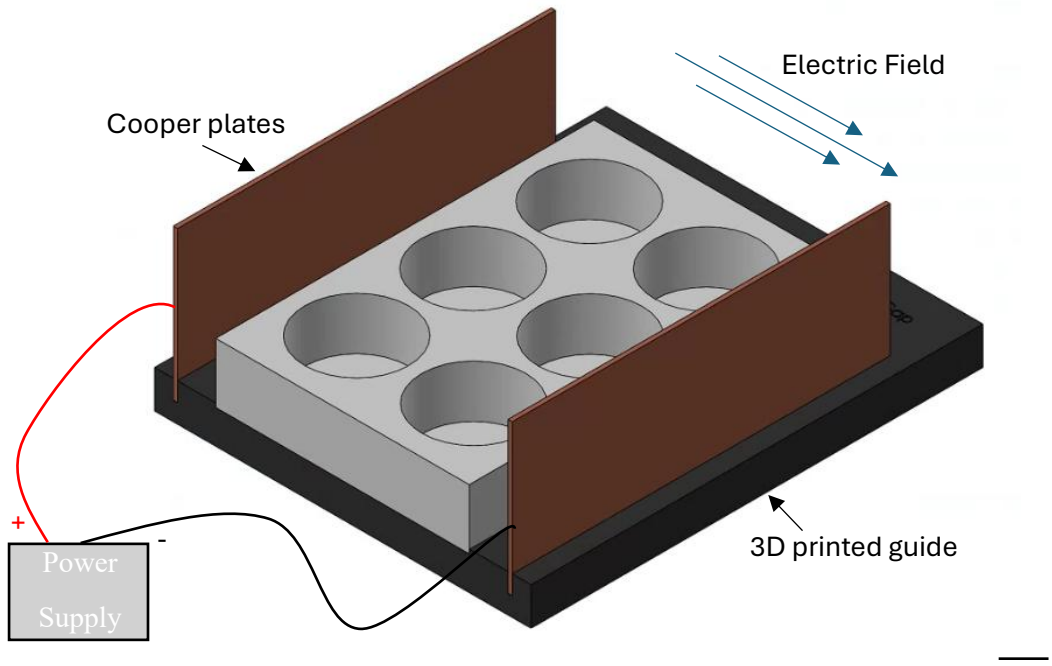

Figure 25: In vitro electric field device. The device was fabricated in three parts, a 3D printed guide that was designed in SolidWorks and printed on a Form 3B+ (Formlabs, Somerville, MA) out of clear resin, and two super conductive copper sheets cut to fit in the 3D printed guides predetermined slots. Scale bar: 13 mm.

3.3 Experimentation

In vitro experiments were conducted on frozen stocks of human mesenchymal stem cells (hMSCs) (Lonza, USA). Cells were recovered and allowed to reach 80% confluency in growth media (DMEM high glucose GLUTAMAX (Gibco), 10 % Fetal Bovine Serum (Gibco), 1% antibiotic-antimycotic (Gibco), 1% Non-Essential Amino Acids (Gibco), and 5ng/mL basic fibroblast growth factor (Gibco)). After recovery and expansion, hMSCs were seeded in either six well plates, for qPCR, and Western Blotting, or 48-well plates, for staining, at a seeding density of 96,000 cells/well and 10,000 cells/well respectively. Two days post seeding, half of the experimental plates were shifted to osteogenic media (DMEM high glucose GLUTAMAX (Gibco), 10% Fetal Bovine Serum (Gibco), 1% antibiotic-antimycotic (Gibco), 100 nM dexamethasone (Sigma-Aldrich), 10 mM sodium β-glycerophosphate (Sigma-Aldrich), and 0.05

mM 1-ascorbic acid) to begin the initial differentiation, while the other half remained on a growth media regiment. Media was changed every 2-3 days for the duration of the study[27].

3.3.1 In vitro EF Treatment

Treatment was performed on two culture groups comprised of growth media and osteogenic media. Plates were treated outside the incubator for 10 minutes daily with approximately 1.5 V/cm[32]. Control plates were not exposed to EF but were removed from the incubator for continuity. Prior to the start of treatment, each well received a scratch through its center to visualize cell migration. Timepoints were collected at 7, 14, 21, and 28 days for control and treatment plates and processed for Live/Dead staining, Western Blotting, qPCR, and Phospho-SMAD staining.

3.4 In vitro Methods

3.4.1 Live/Dead Staining

Live/Dead analysis was performed at 7, 14, 21, and 28 days using an Invitrogen Live/Dead Cell Imaging Kit (Fisher). Kit components were mixed in the dark according to manufactures instruction and diluted in DMEM (Gibco). Media was aspirated from the wells and 0.5 mL of Live/Dead in DMEM was added to each well and incubated at 37ºC and 5% CO_2 for 30 minutes. After incubation, the media was aspirated and replaced with DMEM. Plates were wrapped in tinfoil to prevent light exposure until imaging. Plates were imaged using a BZ-X series Fluorescence Microscope (Keyence, Itasca, IL). Quantification of live/dead staining was done using ImageJ (NIH, Bethesda, MD) and the live/dead quantification add on.

3.4.2 Cryptochrome 1 (CRY1) & Bone morphogenic protein 2 (BMP2) Western Blotting

Western Blot was performed at 7, 14, 21, and 28 days to detect cryptochrome 1 (CRY1) and BMP2 levels of the treatment and control groups. Media was collected and samples were washed 2 times with cold Dulbecco's Phosphate-Buffered Saline (DPBS). DPBS was aspirated

and 100 µL of chilled lysing buffer (1 mL RIPA 10X Lysis Buffer (Millipore Sigma), 9 mL distilled water (Invitrogen), and 1 Pierce Protease and Phosphatase Inhibitor (Thermo Scientific)) were added to each well. A fresh buffer solution was prepared before each timepoint. Wells were scraped using a cell scraper, collected, and kept on ice for 30 minutes with occasional agitation. After 30 minutes, samples were centrifuged at 4ºC and 15,000 RCF for 15 minutes. Supernatant was collected and the pellets were discarded. Samples were kept on ice and moved to a -80ºC freezer for long-term storage.

Samples were placed on ice, allowed to thaw slowly, and prepared with 33 µL of SDS (~ 100 µL sample to 33 µL SDS). The positive control (CRY1 recombinant protein) was thawed and prepared using 10 µL recombinant protein, 90 µL UltraPure DNase/RNase-Free Distilled Water (Invitrogen), and 30 µL SDS. Samples and control were heated at 95ºC for 5 mins prior to gel loading. Ladder (5 µL), samples (30 µL), and positive control (5 µL) were loaded on a Blot 8%, Bis-Tris Plus WedgeWell Gel (Invitrogen) and ran in MES-SDS running buffer (Invitrogen) on a Mini Gel Tank (Invitrogen) at 200 V for 45 minutes. After 45 minutes, gels were removed, and proteins were transferred using a mini nitrocellulose iBlot 2 Transfer Stack (Invitrogen) on an iBlot 2 Gel Transfer Device (Invitrogen) at 20 V for 6 minutes. After transfer, the membranes were removed and trimmed in deionized water. Membranes were placed in 5% BSA and agitated for 1 hour at room temperature. After 1 hour, the 5% BSA was removed and replaced with either diluted (1:2500) CRY1 polyclonal antibody or diluted (1:2000) BMP2 monoclonal antibody and agitated at 4ºC overnight. The primary antibody was removed, and the membranes were washed 3 times in a solution of tris buffered saline and tween 20 (TBST) with agitation for 5 minutes. After washing, diluted secondary antibody was added and agitated for 1 hour at room temperature. The secondary antibody solution was removed, and the membranes were washed with TBST 3 times with

agitation for 5 minutes. Chemiluminescent substrate was prepared according to manufacturer's instruction and added to the membranes for a 1-minute incubation. Membranes were then analyzed using a ChemiDoc Imaging System (Bio-Rad, Hercules, CA).

3.4.3 qPCR

qPCR was performed at 7, 14, 21, and 28 days for the following primers, GapDH, Runx2, Osteopontin (OP), bone sialoprotein (BSP), and BMP2. Samples were collected by first aspirating the media from each well followed by the addition of 350 µL of β-ME Buffer RLT (containing 10 µL of β-ME per 1 mL of Buffer RLT). The wells were scraped and transferred into 2 mL tubes, which were stored at -80°C. For RNA isolation, samples were thawed and pipetted up and down to ensure thorough mixing. Next the samples were transferred to Qiashredder tubes, and centrifuge at ~17,000 g for 2 minutes. Afterward centrifugation, the top portion of the tube was removed and discarded and 350 µL of 70% ethanol was added to each sample. The samples were then transferred into a spin column and centrifuged at ~17,000 g for 15 seconds. The flow-through was discarded and 700 µL of Buffer RW1 was added to the spin column and centrifuge at ~17,000 g for 15 seconds, followed by discarding the flow-through. This step was repeated with the addition of 500 µL of Buffer RPE. Then, an additional 500 µL of Buffer RPE was added and centrifuge at ~17,000 g for 2 minutes. The spin column was then placed into a new 2 mL collection tube and centrifuge at ~17,000 g for 1 minute. Transfer the spin column to a new 1.5 mL collection tube and 35 µL of RNase-free water was added directly onto the column membrane and centrifuged at ~17,000 g for 1 minute. Samples were kept on ice while their purity and quantity was assessed using a NanoDrop (Thermo scientific). The ideal usable readout is above 1.75 for 260/280 and 260/230. Samples were stored at -80°C.

For cDNA synthesis, a High-Capacity cDNA Reverse Transcription kit (Applied Biosystems) was used. First, kit components and samples were thawed on ice and the necessary volumes for the master mix based on the NanoDrop results were calculated. Ideally, 1 µg of RNA should be used to synthesize 1 µg of cDNA. The master mix was mixed and 10 µL was transferred into each tube followed by 10 µL of sample in water. Tubes were sealed and placed on ice prior to thermocycling. A MJ Research PTC-200 Thermal Cycler (Bio-Rad, Hercules, CA) with a pre-programmed cycle was used.

For qPCR, a 96-well plate was prepared by adding 10 µL of PowerUp Green Master Mix (info) to each well, followed by 8 µL of diluted cDNA and 2 µL of predetermined primers per well. The plate was sealed and centrifuged to collect the samples at the bottom and remove any bubbles. Plates were read using a Bio-Rad CFX96 Touch Real-time PCR Detection System (Bio-Rad, Hercules, CA) and a preprogrammed cycle.

3.4.4 Phospho-SMAD staining

Phospho-SMAD staining was performed at 7, 14, 21, and 28 days in accordance with the following protocol. Adherent cell cultures were aspirated and fixed with 200 µL of 4% paraformaldehyde (PFA) for 30 minutes. After which PFA was removed, and samples were washed 3 times with 500 µL of 1X Dulbecco's Phosphate-Buffered Saline (DPBS) (Gibco). Samples were then permeabilized by the addition of 400 µL of 0.1% Triton X-100 in DPBS for 15 minutes at room temperature. After 15 minutes, samples were washed 3 times in 500 µL of DPBS. Next samples were blocked with 2% bovine serum albumin (BSA) in DPBS for 1 hour at room temperature. Aspirated blocking agent was replaced with 500 µL of diluted primary antibody and incubated overnight at 4ºC. Primary antibody was aspirated and washed 3 times with DPBS followed by the addition of 500 µL of secondary antibody for 45 minutes at room temperature

shielded from light. Lastly, secondaries were aspirated and washed 3 times with DPBS. An additional 500 μL of DPBS was added followed by sample imaging with a BZ-X 710 fluorescent microscope (Keyence, Woburn, MA).

3.5 Results and Discussion

Due to time constraints, the data was unable to be completely processed as outlined in the methods section. The following is the preliminary data up to day 14.

Preliminary Live/Dead staining (Figure 26) of the control and electric field treatment groups on day 7 and 14 for growth media and osteogenic media. The results showed no visibly significant cell death in the treatment groups compared to the control groups. Further quantification of the Live/Dead images via ImageJ was attempted using the live/dead quantification plug-in. Unfortunately, due to the stitching of the images, the plug-in could not analyze the images. Visual assessment of the scratch growth particularly in the day 7 growth media showed that the treatment group filled in the gap more than the control group. This was insightful as it showed that the treatment was potentially influencing the cells proliferation rate. By day 14 for growth media, there was no visible difference observed between the control and treatment groups with both completely sealing the gap. With respect to the osteogenic media group, the most visible difference is seen in day 14 treatment group as it appears to be showing early signs of regrowth in the gap space.

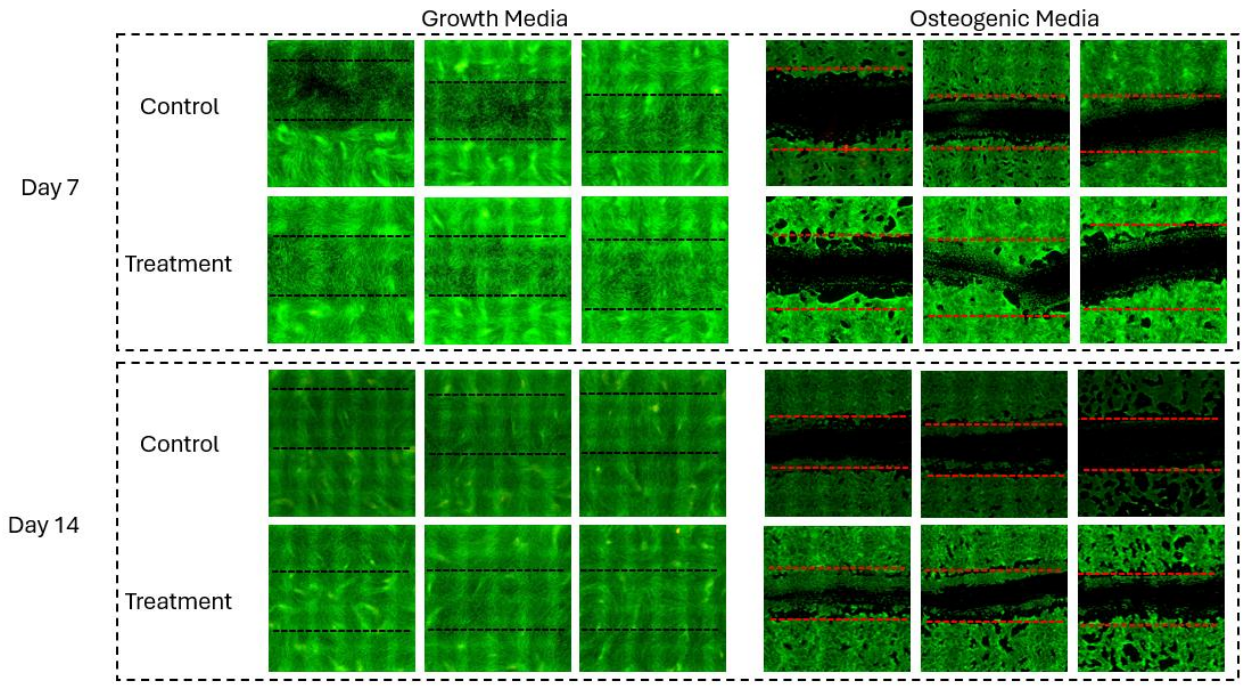

Figure 26: Preliminary Live/Dead staining of control and treatment groups for days 7 and 14. The control group received no electric field treatment, and the treatment groups received 10 minutes of electric field exposure each day. Live cells are shown in green and dead cells are shown in red. The scratched gaps are highlighted with the black and red dashed lines. Images were taken with a BZ-X series fluorescent microscope and stitched together using the accompanying software. Treatment does not show a visible impact on cell viability. Scale bar: 100 microns.

3.6 Device Overview - in vivo

3.6.1 Design and Fabrication

In order to be applicable for in vivo studies, the prior device designed for the EF in vitro studies was scaled up 2-fold to accommodate a mouse enclosure (Figure 27). The guide will be machined out of Clear polycarbonate (McMaster Carr, Elmhurst, IL). The outer dimensions of the guide are 254 mm wide, 306.8 mm long, and 25.4 mm thick. An etch of 171 mm wide, 255.2 mm long, and 2.54 mm deep will be centered to the bottom of the guide for the mouse enclosure placement. The mouse enclosure was cut from polycarbonate (McMaster Carr, Elmhurst, IL). The outer dimensions of the enclosure are 255 mm long, 171 mm wide, and 127 mm tall. The inner dimensions are 248 mm long, 164 mm wide, and 123 mm tall. Superconductive copper plates

(McMaster Carr, Elmhurst, IL) will be cut to the following specifications, 255 mm long, 1.4 mm wide, and 101.6 mm tall. Each copper plate will then be slotted into place on the guide's track 223 mm apart. Power to generate the field will be applied to the cooper plates by a Hanmatek 305T power supply (Hanmatek, Shenzhen, China).

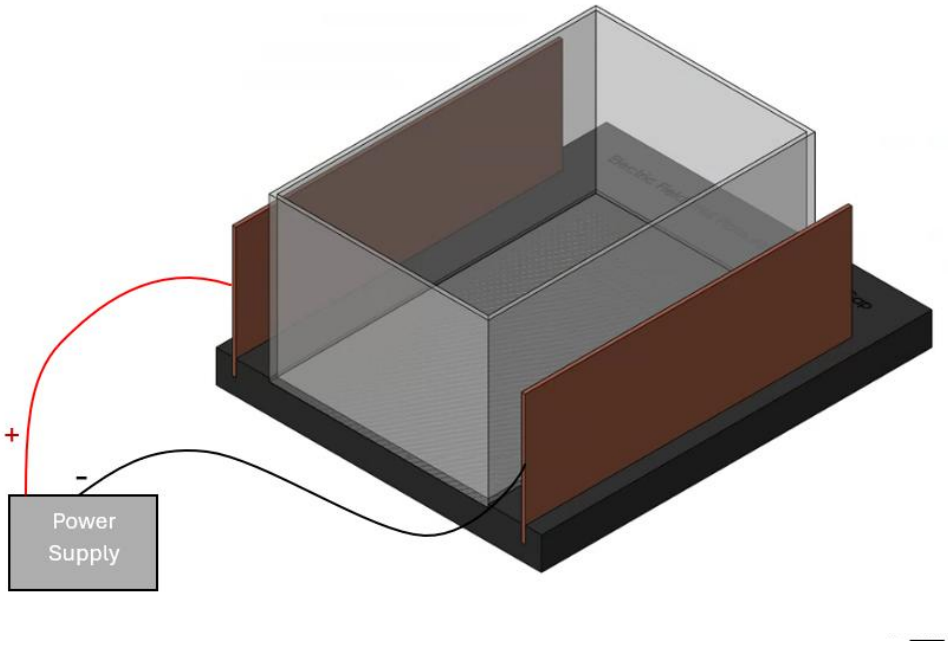

Figure 27: In vivo electric field device. The device was fabricated in three parts, a 3D printed guide that was designed in SolidWorks and printed on a Form 3B+ (Formlabs, Somerville, MA) out of clear resin, and two super conductive copper sheets cut to fit in the 3D printed guides predetermined slots. Scale bar: 26 mm.

3.7 Experimentation

Post amputation bleeding will be minimized by applying mild pressure to the hind paw and the animal will be allowed to wake up and return to its housing enclosure for ~ 1-2 hours. Following the recovery period, animals will be moved from their housing enclosure to the testing enclosure and allowed to acclimate for 15 minutes. After acclimation, EF treatment will be

deployed for 10 minutes. After 10-minute treatment, the animal will be returned to its housing enclosure. EF treatment will be administered every day for 10 minutes over a 28-day period.

3.8 In vivo Methods

In vivo experiments will be conducted on female CD-1 mice (Charles River Laboratories) using custom treatment devices. Since the EF device acts on the subject externally, it does not need to undergo any specific sterilization process. The custom enclosure does require sterilization and can accomplished using 70% ethanol.

3.8.1 Limb Amputation

All surgeries will be approved by Tufts University IACUC under protocol M2022-128. CD-1 mice will be prepared for P2 amputation surgery using standardized protocols. Surgery preparation, under anesthesia, for each animal will be done with a combination of Betadine (Perdue) and alcohol swabs (BD) three times each. Control and treatment animals will receive P2 amputations of right hind paw middle digit under a microscope using a scalpel. Any bleeding will be stopped with mild pressure applied to the digit and a cotton swab. Animals will be returned to their housing enclosures post bleeding reduction.

3.8.2 Histology and Immunostaining

Post treatment, animals will be sacrificed humanely using standard IACUC approved protocols. The digits will be harvested and fixed with 4% paraformaldehyde (PFA) at room temperature for 24 hours. Following PFA fixation, samples will be removed and washed in 1x PBS four times. The samples will be left in the last PBS wash overnight at 4ºC. PBS will be replaced with fresh PBS for 10 minutes followed by the addition of Surgipath decalcifier I for 2 hours. After 2 hours, the decalcifier will be removed and replaced with fresh decalcifier and allowed to sit overnight. Tissues will then be washed 4 times with PBS before undergoing graded ethanol

dehydration. After treating overnight at 4ºC, 100% ethanol solution will be replaced with xylene and placed under vacuum for 1.5 hours (twice). Samples will then be transferred into molten paraffin for infiltration. This will be done twice for 2.5 hours each under vacuum. Samples will then be fully embedded in paraffin and sectioned using a microtome (Leica Biosystems, Nussloch, Germany)[6]. Following sectioning, samples will undergo standard hematoxylin and eosin staining protocols.

3.9 Discussion

Unfortunately, due to time limitations and the intensity associated with animal studies, preliminary studies of this section of the study were not able to be fulfilled. Future studies using this device will be conducted in accordance with the methods outlined above.

3.10 Limitations

The major limitation of this preliminary study was time. Due to time restrictions, study duration as well as methods of analysis had to be significantly cut back. With respect to the treatment device, the initial in vitro system was easy to use and provided a reliably repeatable design. However, field strength readings via electromagnetic field detector (GQ Electronics LLC, Seattle, WA) showed that the device field strength was less than desired. Due to the voltage range limitations of our power supply, I was unable to adjust accordingly to reach the desired field strength.

3.11 Conclusions

An in vitro device was successfully designed and fabricated for the electric field stimulation system. Preliminary in vitro testing showed that our treatment was not inducing any visible negative impact on overall cell health. Additionally, a visible increase in cell proliferation

into the induced scratch gap was observed in the growth media treatment group compared to the control group of the same media and time point.

3.11.1 Future Directions

To build upon the preliminary in vitro electric field work, expanding the study out to the full 28-day experimental period is necessary to better assess any potential health impacts caused to the cells by the treatment. Additionally, modifying the scratch component of the study to include other directions or half well removal may result in better visualization of the migration patterns induced by the electric fields. In addition to the analyses listed above, testing for neurogenic markers would be insightful as reinnervation is another critical component of regeneration and electrical-based stimulation methods have been shown to enhance nerve regeneration[12]. Further testing and analysis of the first iteration device is necessary to determine if the current device configuration is the most optimal for administering treatment. Additional device configurations can be explored, such as a copper coil tube, to see if changing the method in which the treatment is administered has an effect on the treatments outcome biologically.

Exploration of different field strengths would be insightful in that it may result in different levels of regeneration. For example, the chosen field strength for this preliminary study has been shown to be an effective strength for skin wound healing. If a set of optimal field strengths can be tested for nerve, bone, and muscle regeneration, some of which may have overlap, a secondary iteration of the device could be designed to pulse through all these strengths allowing multiple levels to be affected at once.

Lastly, the in vivo component of this chapter requires the most work as it has yet to undergo any preliminary studies. Device fabrication and logistic work are the primary steps that must occur to get this study off the ground. After those are established, testing of continuous and pulsed

electric fields would be critical as it would allow for insight into the first iteration devices functionality. An initial concern is that the animal's constant motion within the treatment enclosure seen in Figure 27 would influence how the electric field directs cell migration. Being able to better understand this and the results the treatment directly has on the tissue would allow for a fine-tuned device to be designed and fabricated.

Chapter 4: Additional Research Device Development for the Biodome

4.1 Introduction

The Biodome project's goal is to develop methodologies to promote improved healing and regeneration of tissues. Not only does the project focus on the enhanced regeneration of limbs for non-regenerative species, but it also investigates other models such as skin. To generate a multilayer skin model, I developed two miniaturized systems based off the work of Pappalardo et al. to facilitate the generation of the multilayer model and the subsequent testing of the model in a sterile air environment[33].

4.2 Device Overview

4.2.1 Design and Fabrication

The first stage of this system focused on the attachment and culturing of skin cells. To do this, a custom scaffold was designed in Solidworks (Dessault Systemes, Waltham, MA) and printed using a Formlabs Form3B+ SLA print (Formlabs, Somerville, MA) out of IBT Flex resin (Formlabs, Somerville, MA). This resin was chosen as its properties best matched that of the material used by Pappalardo et al.[33] The scaffold (shown in Figure 28) is hollow throughout with 0.6 mm pores spaced 1 mm apart to allow for internal media perfusion. The scaffold is 31 mm long and 7 mm at the widest point with a wall thickness of 0.7 mm. The scaffold is contained within a 3D printed culture chamber that consists of two soft inner components and 2 rigid outer components. The inner components were printed out of Biomed Flex 80A resin (Formlabs, Somerville, MA) due to its biocompatibility properties and ease of sterilization while the outer components were printed from Biomed Clear resin (Formlabs, Somerville, MA) also for its biocompatibility and sterilization properties. The scaffold is suspended within the inner chamber via the perfusion nozzles. The device is easy to assemble and maintains a liquid tight seal due to

compression of the soft inner chamber by the rigid outer lids. The culture chamber is 45 mm long, 20 mm wide, and 30 mm tall. The CAD model of this device is shown in Figure 28 a and b, and a fully fabricated prototype is shown in Figure 28c.

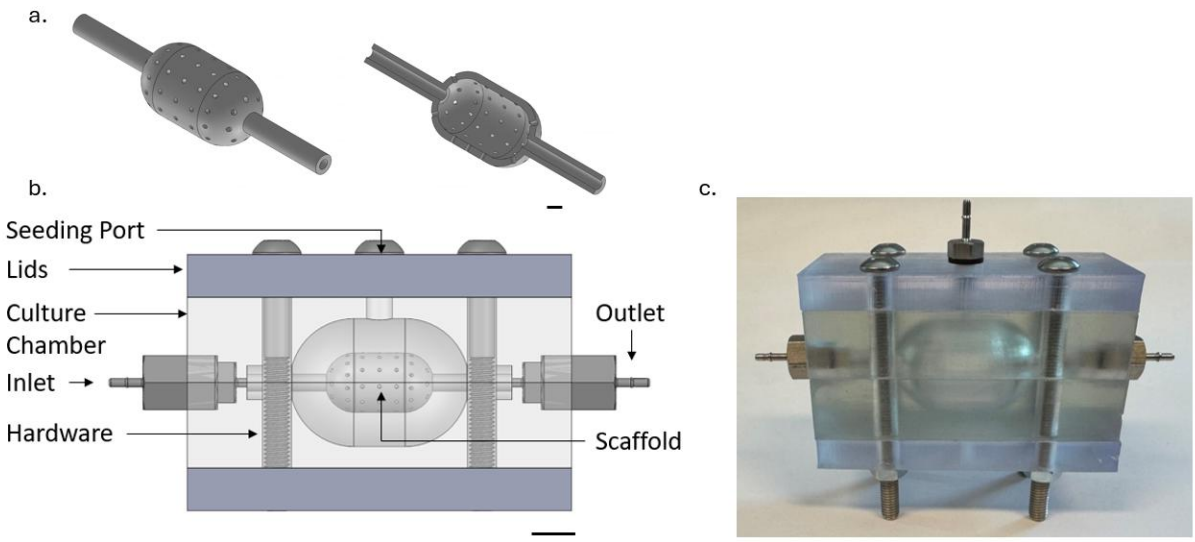

Figure 28: CAD model of the scaffold (a). The scaffold was designed in Solidworks and is 31 mm long and 7 mm at the widest point. The scaffold is designed to be hollow and porous to allow for media perfusion. The resulting wall thickness is 0.7 mm and the pore diameter is 0.6 mm with a 1 mm space in between each. Scaffolds were 3D printed on a Form3B+ from IBT Flex resin. The 3D printed culture chamber (b) is constructed of four main components, 2 rigid lids and 2 soft inner chambers. The rigid lids were printed from Biomed Clear resin and the soft inner chamber was printed from Biomed Flex resin. The scaffold is suspended within the center of the device via the perfusion nozzles. Bolting of the 2 rigid lids to each other results in a liquid tight seal to be formed. (c) Image of a single fabricated and assembled device. Scale bar: (a) 2 mm, (b) 5 mm.

After the initial culture period, cell-laden scaffolds are removed from the culture chamber and transferred to air chambers (Figure 29). The purpose of the air chamber is to provide a sterile environment to test the integrity of the skin layers. These chambers were designed in Solidworks (Dessault Systemes, Waltham, MA) and printed from biocompatible resin (Biomed Clear) in a Form3B+ SLA printer (Formlabs, Somerville, MA). The chamber's outer dimensions are 50 mm long, 25 mm wide, and 25 mm tall. The inner dimensions are 40 mm long, 15 mm wide, and 15

mm tall. The scaffold is supported within the chamber and suspended off the bottom of the chamber by the perfusion nozzles. The chamber is liquid sealed via O-rings and silicone sheets at the nozzle interface and the lid interface respectively. An air port was added in the lid and allows for the connection of a luer lock filter (not shown) for sterile airflow within the system.

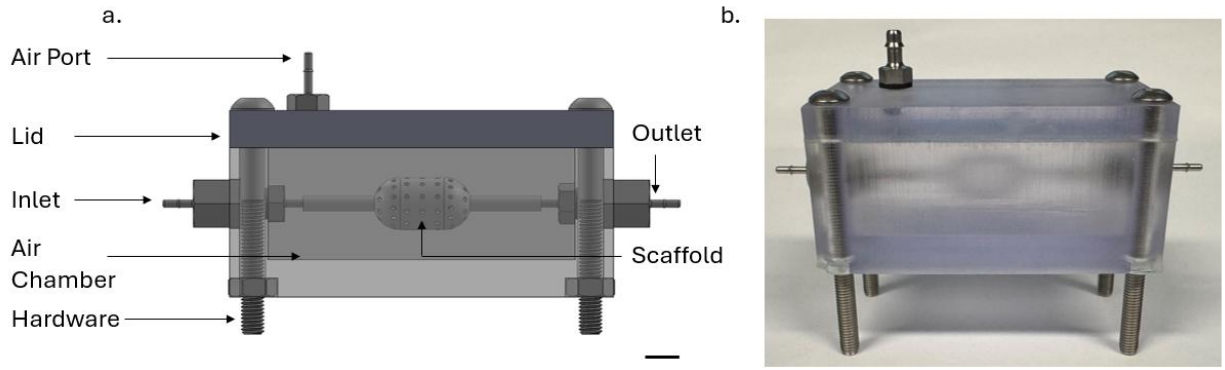

Figure 29: CAD model of the fully assembled air chamber system designed in Solidworks (a). The external dimensions of the system are 50 mm long, 25 mm, wide and 25 mm tall. The inner dimensions are 40 mm long, 15 mm wide, and 15 mm tall. The chamber and lid are 3D printed on a Form3B+ from Biomed Clear resin. Scaffolds are centered and supported by attached perfusion nozzles. An airport through the lid of the system allows for sterile airflow via a luer lock filter (not shown). O-rings and silicone sheets are used to liquid seal the system. (b) Image of a single fabricated and assembled device. Scale bar: 5 mm

4.3 Conclusions

Fabrication of the scaffolds had its initial challenges due to the size of the pores, which tended to clog with residual resin and therefore unusable. This was amended by switching from a mild agitation wash to a sonicating wash. Additional device components printed smoothly and assembled easily.

Unfortunately, these devices are in their early stages of development and have not yet been used for experimentation. However, they are currently being bulk produced for anticipated experimentation in the new year.

Chapter 5: Conclusions

5.1 Research Summary

The work laid out in this thesis was directed toward the development of enhanced regenerative abilities in a non-regenerative model by non-invasive stimulation methods. Chapter 1 highlighted the necessity for this as to date the current options for individuals with limb loss is providing a low or high functioning replacement limb. These devices come at a cost and can be challenging to work with for younger individuals as they are not fully matured. Prosthetics also come with the limitation that they primarily appear as a foreign object on the body which can result in poor acceptance by the user both physically and mentally. Our research focus is ideal for combatting both these physical and mental rejections as it would allow for both functionality and the individual's ability to feel whole.

Chapter 2 walked through the first attempted method of enhanced regeneration, optical stimulation. The focus of this chapter was the use of 810 nm wavelength light to natively interact with the cells and tissues to promote regeneration. This method and wavelength were chosen as it is non-invasive and has a large penetration depth. Research into this wavelength also showed its prior use in bone regeneration which also made it an ideal starting point. Although issues were encountered with some delivery methods and data analysis, the data collected showed promise that exposure to this wavelength of light did not cause any harm at the cell or tissue level and in fact may promote better wound healing.

Chapter 3 walked through using electric fields as a stimulation method for enhanced regeneration. The focus of this chapter was the use of a 1.5 V/cm strength electric field to guide cell migration across an induced wound in vitro. This method was chosen as it is a non-invasive method that correlates to the naturally occurring wound healing methods of the body. The field

strength chosen was based upon prior research that showed that this strength had an influence on skin wound healing. Although a complete study and analysis was not able to be completed, preliminary data showed interesting results that could be indicative of enhanced proliferation as well as potentially minimal effects on viability.

Chapter 4 took a step away from the main objectives of this project and explored the design and fabrication of systems to generate a multilayer skin model. These devices are still in their infancy but hold promise for further research and development within the Biodome project.

The objectives outlined in section 1.2 have all been addressed and tested in the scope of the project. An optical stimulation system to enhance regeneration was fabricated and tested in vitro and in vivo and showed promise in the use of non-invasive light therapy as a potential option for enhancing the health and potential regeneration at the amputation site. An electric field-based stimulation system was also fabricated and underwent initial in vitro testing.

5.2 Novel Contributions

The novelty of this research is the combination of multiple forms of non-invasive stimulation that can work together to enhance aspects of regeneration and wound health in their own ways. The work done in this thesis was primarily to build out and justify the chosen stimulation methods as options for a larger collaborative. With the results obtained, future work to build a device that encompasses all methods can be developed for testing.

5.3 Future Directions

There are numerous possibilities for future work around this project. With respect to optical stimulation, improvements to the reliability of the devices can be made. These improvements, which could include the use of a wired single optical fiber system or a wrap of 2D sheet LEDs within the cast, would allow for more reliability in vivo data collection and exposure, which would

allow for a better understanding of the treatment at the tissue level. Additionally, alternative wavelengths, time durations, intensities, and delivery mechanisms (continuous vs pulsed) can be explored to develop the most optimized version of treatment. When thinking about the human scale of this treatment, optimization in favor of time is ideal as it would result in minimal additional impact on the patient's day-to-day life. Therefore, by tuning the intensity and/or surrounding the wound site in a pulsing light tunnel, the time the patient would need to wear the treatment devices may be able to be shortened immensely.

The same can be said for the electric field stimulation as optimization is the highest priority in the development of a therapeutic device. Though much at this time is still unknown for the electric field treatment, more work in understanding its fundamental effect through preliminary in vitro and in vivo studies is necessary. Once established improvements on the devices and optimization of the treatment can be made.

Once fully optimized, the development of a unified system of optical, electrical, and pharmaceutical (prior group work) would be the next major step in this project's advancement as understanding how these systems interact together is key. For in vitro studies, testing could be conducted using the established devices with minimal modifications. Based on the results obtained in vitro and after establishing if any of the devices negatively interfere with one another, modifications can be made to establish initial in vivo testing devices.

On the more fundamental side of this project, understanding the biological mechanisms of how optical and electrical stimulation interact at the cellular level is also of high interest. Much work in the field has implied that these methods may be interacting with the ion channels. Methods to analyze these interactions could make use of patch-clamp systems or voltage-sensitive dyes during treatment to map the ion channels activities.

References

1. 29 Limb Loss Statistics, Facts & Demographics – Pro Medical East. https://promedeast.com/limb-loss-statistics/ (2023).
2. Ziegler-Graham, K., MacKenzie, E. J., Ephraim, P. L., Travison, T. G. & Brookmeyer, R. Estimating the prevalence of limb loss in the United States: 2005 to 2050. *Arch Phys Med Rehabil* **89**, 422–429 (2008).
3. Manero, A. *et al.* Implementation of 3D Printing Technology in the Field of Prosthetics: Past, Present, and Future. *Int J Environ Res Public Health* **16**, 1641 (2019).
4. Perry, B. N. *et al.* Initial Clinical Evaluation of the Modular Prosthetic Limb. *Front Neurol* **9**, 153 (2018).
5. Petrini, F. M. *et al.* Sensory feedback restoration in leg amputees improves walking speed, metabolic cost and phantom pain. *Nat Med* **25**, 1356–1363 (2019).
6. Murugan, N. J. *et al.* Acute multidrug delivery via a wearable bioreactor facilitates long-term limb regeneration and functional recovery in adult Xenopus laevis. *Sci Adv* **8**, eabj2164 (2022).
7. Peng, J. *et al.* Low intensity near-infrared light promotes bone regeneration via circadian clock protein cryptochrome 1. *Int J Oral Sci* **14**, 1–11 (2022).
8. Hu, W. *et al.* Optogenetics sheds new light on tissue engineering and regenerative medicine. *Biomaterials* **227**, 119546 (2020).
9. Sanchez-Casanova, S. *et al.* Local delivery of bone morphogenetic protein-2 from near infrared-responsive hydrogels for bone tissue regeneration. *Biomaterials* **241**, 119909 (2020).
10. Hechavarria, D., Dewilde, A., Braunhut, S., Levin, M. & Kaplan, D. L. BioDome regenerative sleeve for biochemical and biophysical stimulation of tissue regeneration. *Med Eng Phys* **32**, 1065–1073 (2010).

11. Zhao, M. Electrical fields in wound healing-An overriding signal that directs cell migration. *Semin Cell Dev Biol* **20**, 674–682 (2009).
12. Leppik, L. P. *et al.* Effects of electrical stimulation on rat limb regeneration, a new look at an old model. *Sci Rep* **5**, 18353 (2015).
13. Oliveira, K. M. C. *et al.* Electrical stimulation shifts healing/scarring towards regeneration in a rat limb amputation model. *Sci Rep* **9**, 11433 (2019).
14. Cezar, C. A. *et al.* Biologic-free mechanically induced muscle regeneration. *Proc Natl Acad Sci U S A* **113**, 1534–1539 (2016).
15. Suckow, M. A., Voytik-Harbin, S. L., Terril, L. A. & Badylak, S. F. Enhanced bone regeneration using porcine small intestinal submucosa. *J Invest Surg* **12**, 277–287 (1999).
16. Zhang, R. & Qu, J. The Mechanisms and Efficacy of Photobiomodulation Therapy for Arthritis: A Comprehensive Review. *International Journal of Molecular Sciences* **24**, 14293 (2023).
17. Syed, S. B. *et al.* Photobiomodulation Therapy Mitigates Cardiovascular Aging and Improves Survival. *Lasers in surgery and medicine* **55**, 278 (2023).
18. Malavazzi, T. C. dos S. *et al.* Preventive and therapeutic vascular photobiomodulation decreases the inflammatory markers and enhances the muscle repair process in an animal model. *Journal of Photochemistry and Photobiology B: Biology* **256**, 112921 (2024).
19. Barolet, D. Light-emitting diodes (LEDs) in dermatology. *Semin Cutan Med Surg* **27**, 227–238 (2008).
20. Parico, G. C. G. *et al.* The human CRY1 tail controls circadian timing by regulating its association with CLOCK:BMAL1. *Proceedings of the National Academy of Sciences* **117**, 27971–27979 (2020).

21. Narasimamurthy, R. *et al.* Circadian clock protein cryptochrome regulates the expression of proinflammatory cytokines. *Proceedings of the National Academy of Sciences* **109**, 12662–12667 (2012).
22. Zhou, W. *et al.* Endogenous Parathyroid Hormone Promotes Fracture Healing by Increasing Expression of BMPR2 through cAMP/PKA/CREB Pathway in Mice. *Cell Physiol Biochem* **42**, 551–563 (2017).
23. Wang, C. *et al.* Defect-Related Luminescent Hydroxyapatite-Enhanced Osteogenic Differentiation of Bone Mesenchymal Stem Cells Via an ATP-Induced cAMP/PKA Pathway. *ACS Appl Mater Interfaces* **8**, 11262–11271 (2016).
24. Maes, C. Signaling pathways effecting crosstalk between cartilage and adjacent tissues: Seminars in cell and developmental biology: The biology and pathology of cartilage. *Seminars in Cell & Developmental Biology* **62**, 16–33 (2017).
25. Zhou, L. *et al.* Cryptochrome 1 Regulates Osteoblast Differentiation via the AKT Kinase and Extracellular Signal-Regulated Kinase Signaling Pathways. *Cell Reprogram* **21**, 141–151 (2019).
26. Cai, H., Zou, J., Wang, W. & Yang, A. BMP2 induces hMSC osteogenesis and matrix remodeling. *Molecular Medicine Reports* **23**, 125 (2020).
27. Fitzpatrick, V. *et al.* Functionalized 3D-printed silk-hydroxyapatite scaffolds for enhanced bone regeneration with innervation and vascularization. *Biomaterials* **276**, 120995 (2021).
28. Hamblin, M. R., Carroll, J. D., De Freitas, L. F., Huang, Y.-Y. & Ferraresi, C. *Low-Level Light Therapy: Photobiomodulation*. (SPIE, 2018). doi:10.1117/3.2295638.
29. Fodstad, H. & Hariz, M. Electricity in the treatment of nervous system disease. *Acta Neurochir Suppl* **97**, 11–19 (2007).
30. 2 - Fundamentals of Electric Fields. in *Electromagnetics Explained* (ed. Schmitt, R.) 25–49 (Newnes, Burlington, 2002). doi:10.1016/B978-075067403-4/50003-3.

31. Farber, P. L., Isoldi, F. C. & Ferreira, L. M. Electric Factors in Wound Healing. *Adv Wound Care (New Rochelle)* **10**, 461–476 (2021).
32. Ryan, C. N. M., Doulgkeroglou, M. N. & Zeugolis, D. I. Electric field stimulation for tissue engineering applications. *BMC Biomedical Engineering* **3**, 1 (2021).
33. Pappalardo, A. *et al.* Engineering edgeless human skin with enhanced biomechanical properties. *Sci Adv* **9**, eade2514 (2023).